Journal of Sound and Vibration 329 (2010) 2218–2240

Contents lists available at ScienceDirect

Journal of Sound and Vibration

journal homepage: www.elsevier.com/locate/jsvi

# Dynamic buckling of columns by biaxial moments and uniform end torque

A.Y.T. Leung *

*Building and Construction, City University of Hong Kong, Hong Kong*

ARTICLE INFO

*Article history:*
Received 6 August 2007
Received in revised form
13 November 2009
Accepted 6 December 2009
Handling Editor: L.G. Tham
Available online 12 January 2010

ABSTRACT

A new concept of uniform torque is proposed for the dynamic torsional buckling analysis. A dynamic biaxial moments and torque buckling theory is presented for analysis in structural dynamics. Second-order effects of the axial force, biaxial moments and torque are considered. The consistent natural boundary moments and forces are derived to ensure the symmetry of the dynamic stiffness matrix in fulfilling the requirement of the reciprocal theorem and conservation of energy. The exact dynamic stiffness matrix is obtained using power series expansion. The derivatives of the analytical dynamic stiffness matrix with respect to different loading and geometric parameters are derived explicitly for sensitivity and continuation analyses. Generally distributed axial force can be analyzed without difficulty. It is pointed out that non-uniform sections may not be handled by power series due to the convergent problem. Global pictures for all kinds of linear dynamic buckling are given for the first time. The methodology is based on finite element formulation and therefore it can easily be extended to analyze structural frames.



## 1. Introduction

The rigid body concept proposed by Yang and Kuo [1] is important in nonlinear structural analysis for reducing a nonlinear problem to a series of linear problems. The stability of a curved beam can also be adequately analyzed by straight beam finite elements if the rigid body principle is observed. The initial stresses induced by the internal forces and moments in a structural member must be accurately determined in each linear step within a nonlinear analysis to ensure convergence. Stress induced by initial torque (or torsion) has a long history. Ziegler [2] introduced the concept of quasi- and semi-tangential torque for circular shafts. Argyris et al. [3] generalized it to rectangular sections of unequal principal moments of area. The interested readers are recommended to find an exhaustive list of references in the topic in [1]. The linear beam buckling theory has no further advancement since then.

In this paper, a new concept of uniform torque is proposed for the dynamic torsional buckling analysis. A dynamic biaxial moments and torque buckling theory is presented for analysis in structural dynamics. Second-order effects of the axial force, biaxial moments and torque are considered. The consistent natural boundary moments and forces are derived to ensure the symmetry of the dynamic stiffness matrix in fulfilling the requirement of the reciprocal theorem and conservation of energy. The exact dynamic stiffness matrix is obtained using power series expansion. The derivatives of the analytical dynamic stiffness matrix with respect to different loading and geometric parameters are derived explicitly by

* Tel.: +852 2788 7600; fax: +852 2788 7612.
*E-mail address:* Andrew.leung@cityu.edu.hk

0022-460X/$ - see front matter © 2009 Elsevier Ltd. All rights reserved.
doi:10.1016/j.jsv.2009.12.008

means of the Leung theorem for sensitivity and continuation analyses. The buckling torque is defined as the torque that causes linear instability of the column. A simple engineering application is the prevention of using excessive torque in spanners.

The paper is organized in 12 sections. After an introduction in Section 1, the semi- and quasi-tangential torque in torsional buckling analysis is revisited and compared in detail in Section 2. The deficiency of these concepts is discussed and a new concept of uniform application of the torque over the entire area at the end of the column is introduced. The shear strain components induced fit well with the classical linear torsion theory. In Section 3, the strain energy stored in the column due to the initial torque and biaxial moments is given by means of weak formulation [4]. One advantage of the weak formulation is that nonlinear strain components are avoided. The formulation is much simpler and is less prone to errors. Matrix multiplications and integrations only are required. The total potential energy is given in Section 4. The matrix governing equations and the associated natural boundary conditions are derived by variational principle for non-uniform cross-sections. The equations are then specialized for uniform cross-sections. The governing equations and the associated boundary conditions are given explicitly in Section 5 and the analytical solutions of the governing equations for general boundary conditions are obtained using power series method [5–13] in Section 6. The equations and boundary conditions are then non-dimensionalized with only two structural parameters to define the geometry of the column. These geometric parameters are the rigidity ratio $e=EI_x/EI_y$ and the torsion-warping ratio $K=GJl^2/(r^2EI_y)=GJl^2/(EI_\varpi)$ where $r^2=I_\varpi/I_y$. An additional parameter is also required to handle the rotational inertia $g=J/Ar^2$. These parameters will be explained in detail in Section 6. Explicit formulae are given for the displacement functions which are the analytical solutions of the governing set of ordinary differential equations with unknown integration constants to be determined by the displacement boundary conditions. Once these integration constants are found in terms of the displacement boundary conditions, one obtains the analytical shape functions. The dynamic stiffness matrix can then be formed either by the finite element method or the force method. The force method will be formulated in detail. Section 7 is devoted to the formulation of non-uniformity along the column length. It is found that the power series method is not suitable for non-uniform cross-section due to convergence problem. As the resulting problem is nonlinear with respect to the eigenvalue, solution methods based on Newtonian iteration are inevitable. In order to do so, the partial derivatives of the stiffness matrix with respect to the loading parameters $(\omega^2,P,L,M,N)$ to give the exact mass matrix, axial stability matrix, torque stability matrix and biaxial moment stability matrix, respectively, are required. These matrices can be obtained explicitly by an extension of the Leung theorem [14,15] in Section 8 and the matrices are given in Section 9. The initial approximate natural frequencies without loading can be obtained by the solutions of a linear eigenvalue problem. These initial approximations can be improved by inverse iteration or subspace iteration for cluster eigenvalues. The resulting multi-parameter eigenvalue problem to determine the multi-buckling loads is discussed in Section 10. Extensive numerical examples are given in Section 11 for a thin walled column and a two-section column. The resulting buckling torques for various theories are compared and it is found that the semi-tangential torque over-estimates the buckling torque and the quasi-tangential torque under-estimates it to large extent. Three-dimensional interactive buckling surfaces are given and the various buckling phenomena are discussed. The paper is concluded in Section 12 with some remarks.

## 2. Semi- and quasi-tangential torque

Fig. 1 shows a torque $L$ about the neutral axis $z$ applying at the end of a cantilever column. Classically, there are two ways to apply the torque. One is quasi-tangential when a fictitious rigid rod is welded along the $x$- or $y$-axis and a pair of equal and opposite forces is applied at the two ends of the rod to produce the resultant torque as shown in Fig. 2(a).

The other is semi-tangential when two fictitious rigid rods are welded orthogonally along the $x$- and $y$-axis and two pairs of equal and opposite forces are applied at the four ends of the rods to produce the resultant torque as shown in Fig. 2(b). The quasi-tangential torque induces either shear stress (i) $\tau^0_{zx}=-yL/I_x$ and $\tau^0_{zy}=0$ or (ii) $\tau^0_{zy}=xL/I_y$ and $\tau^0_{zx}=0$ depending on the direction of the fictitious rigid rod, all other stress components are zero. Here, $I_x=\int y^2\,dA$ and $I_y=\int x^2\,dA$ are the principal moments of cross-sectional area $A$. In both case, static equilibrium $L=\int(x\tau^0_{zy}-y\tau^0_{zx})\,dA$ is

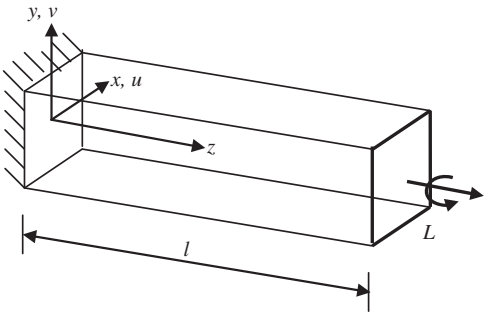


**Fig. 1.** A cantilever subject to an applied torque.

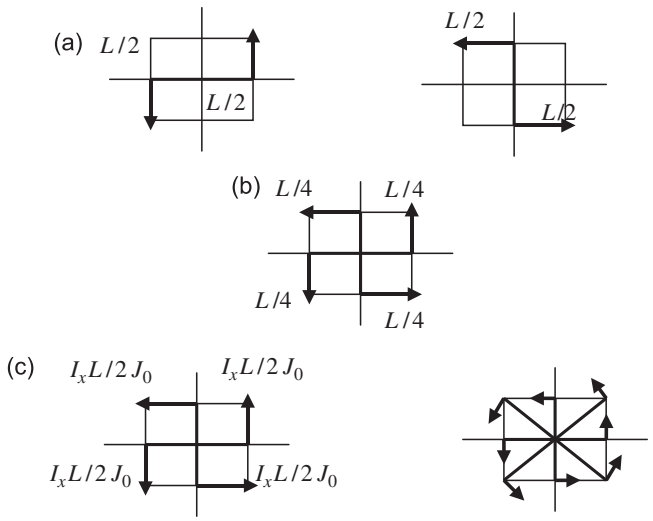


**Fig. 2.** Semi- and quasi-tangential torque (a) Quasi-tangential torque I & II; (b) Semi-tangential torque; (c) uniform torque.

satisfied. The shear strains produced are either (i) $\gamma^0_{zx}=-yL/GI_x$ and $\gamma^0_{zy}=0$ or (ii) $\gamma^0_{zy}=xL/GI_y$ and $\gamma^0_{zx}=0$, for shear modulus $G$. The semi-tangential torque induces shear stress components $\tau^0_{zx}=-yL/2I_x$ and $\tau^0_{zy}=xL/2I_y$ with the corresponding shear strains $\gamma^0_{zx}=-yL/2GI_x$ and $\gamma^0_{zy}=xL/2GI_y$. Static equilibrium $L=\int(x\tau^0_{zy}-y\tau^0_{zx})\,dA$ is also satisfied. The shear flow strength, which is defined as the magnitude of shear stress per unit distance from the centroid per unit applied torque, is given by $(1/I_x,0)$ or $(0,1/I_y)$ for quasi-tangential torque and by $(1/2I_x,1/2I_y)$ for semi-tangential torque. Note that, in both cases, the shear flow strength is non-isotropic that is direction dependent. In real life, it is difficult to determine how much the torque is applied in which direction. Also, it is difficult to define the induced shear stress in an oblique direction, say an arbitrary angle to the $x$-axis when the torque is either quasi- or semi-tangential. Since these torques are self-equilibrating, the stress distribution far away from the end is not affected according to the Saint Venant principle.

An alternative way is to weld a fictitious plate on the whole cross-sectional area at the end of the cantilever and apply the torque uniformly over the entire surface so that $\tau^0_{zy}=xL/J_0$ and $\tau^0_{zx}=-yL/J_0$ where the polar moment of area $J_0=I_x+I_y$. The shear flow strength $(1/J_0,1/J_0)$ is uniform in all directions, i.e., isotropic. For solid sections and closed thin walled sections, the polar moment of area is approximately equal to the torsional constant $J$. The shear strains thus produced are $\gamma^0_{zy}=xL/GJ_0$ and $\gamma^0_{zx}=-yL/GJ_0$ which fit in well with the classical theory that the shear strain of a solid section is proportional to the distance from the centroid alone no matter what the direction is. Now, the shear strain is $\gamma^0=rL/GJ_0$ at a point of distance $r$ from the centroid with no preference of direction. We shall call it the uniform torque, as shown in Fig. 2(c). For easy comparison to the quasi- and semi-tangential torques, the uniform torque is hypothetically drawn on the left of Fig. 2(c) as forces applying at the four ends of two fictitious rods. Physically, the uniform torque applies on the whole cross-section in all directions uniformly as demonstrated on the right of Fig. 2(c). The non-vanishing initial shear stresses satisfy the identity $L=\int(x\tau^0_{zy}-y\tau^0_{zx})\,dA=((I_x+I_y)/J_0)L$.

We shall study the strain energy contained in the column due to the applied torque by various ways of application. Let the displacement vector at a point $(x,y)$ away from the neutral axis be

$$\mathbf{u}=\begin{Bmatrix}u_x\\u_y\\u_z\end{Bmatrix}=\begin{Bmatrix}w-xu'-yv'\\u-y\theta\\v'+x\theta\end{Bmatrix}$$

where $u$, $v$, $w$ are the displacement components of the neutral axis and the angle of twist be $\theta$. The displacement gradient in vector form is given by

$$\overline{\nabla}\mathbf{u}=\begin{Bmatrix}\mathbf{u}_{,x}\\\mathbf{u}_{,y}\\\mathbf{u}_{,z}\end{Bmatrix},\quad \mathbf{u}_{,x}=\frac{\partial\mathbf{u}}{\partial x}=\begin{Bmatrix}-u'\\0\\\theta\end{Bmatrix},\quad \mathbf{u}_{,y}=\begin{Bmatrix}-v'\\-\theta\\0\end{Bmatrix}\quad\text{and}\quad \mathbf{u}_{,z}=\begin{Bmatrix}w'-xu''-yv''\\u'-y\theta'\\v'+x\theta'\end{Bmatrix}\tag{1}$$

where a comma subscript denotes partial differentiation. The strain energy due to initial stresses $\tau^0_{ij}$ for $i,j=x,y,z$ are given by, for example, Washizu [4],

$$U_\sigma=\frac{1}{2}\sum_{i,j=x,y,z}\int\int\tau^0_{ij}\mathbf{u}_{,i}^{\mathrm{T}}\mathbf{u}_{,j}\,dA\,dz\tag{2}$$

For quasi-tangential torque, either $U_{\sigma q}=\int Lu''v'\,dz$ or $U_{\sigma q}=\int -Lu'v''\,dz$. For semi-tangential torque, $U_{\sigma s}=\int \frac{1}{2}L[u''v'-u'v'']\,dz$. Finally, for uniform torque,

$$U_\sigma=\int\left[\frac{LI_y}{J_0}u''v'-\frac{LI_x}{J_0}u'v''\right]dz$$

The share of $L$ is $I_x$:$I_y$ which becomes 1/2:1/2 only when $I_x=I_y$. The strain energy $U_\sigma$ for a beam element shown in Fig. 1 when subject to initial stress caused by initial torque $L$ was proposed by Zeigler [2] when $I_x$=$I_y$ where the sharing is obviously 1/2:1/2. The equal share cannot be generalized to the situation when $I_x\neq I_y$ when the torque is uniformly applied. The significance of the sharing is illustrated in the following torque buckling problem.

Using the principle of minimum total potential energy, the governing equations are:

$$EI_xv''''+Lu'''=0,\quad EI_yu''''-Lv'''=0$$

with natural boundary forces

$$\overline{Q}_v=-EI_xv'''-Lu'',\quad \overline{Q}_u=-EI_yu'''+Lv''$$

and natural boundary moments

$$\overline{M}_v=EI_xv''+\frac{LI_x}{J}u',\quad \overline{M}_u=EI_yu''-\frac{LI_y}{J}v'$$

Assign the sharing factor $\alpha=I_y/J$ to study its significance so that

$$\overline{M}_v=EI_xv''+(1-\alpha)Lu',\quad \overline{M}_u=EI_yu''-\alpha Lv'$$

The displacement functions for a cantilever satisfying all conditions, i.e., the governing equations, the displacement conditions at the clamped end $x$=0 and the natural boundary forces at $x$=$l$=1, except the natural boundary moments at $x$=$l$=1 are given by

$$v=(\sin kz-kz)c_1-(1-\cos kz)c_2,\quad u=(1-\cos kz)rc_1+(\sin kz-kz)rc_2$$

where

$$k=L/\sqrt{EI_xEI_y}\quad\text{and}\quad r=\sqrt{EI_x/EI_y}$$

Substituting the displacement functions in the natural boundary moments at $x$=$l$=1, one has two linear homogeneous equations for $c_1$ and $c_2$:

$$\frac{\overline{M}_v}{EI_x}=v''+(1-\alpha)\frac{L}{EI_x}u'=v''+(1-\alpha)\frac{k}{r}u'=0,\quad \frac{\overline{M}_w}{EI_y}=u''-\alpha\frac{L}{EI_y}v'=u''-\alpha krv'=0$$

or

$$\begin{bmatrix}\alpha+(1-\alpha)\cos k & -(1-\alpha)\sin k\\ -\alpha\sin k & -1+\alpha-\alpha\cos k\end{bmatrix}\begin{Bmatrix}c_1\\c_2\end{Bmatrix}=0$$

The vanishing of the determinant gives the determining equation for $k$

$$2\alpha(1-\alpha)+(1-2\alpha+2\alpha^2)\cos k=0$$

When $\alpha=0.5$, one obtains the buckling torque of Ziegler [2]

$$L=\pi EI$$

for $I_x=I_y$ and $l$=1. However, when $I_z\neq I_y$, then $L=\beta\pi\sqrt{EI_xEI_z}$, where $\beta=\frac{1}{\pi}\cos^{-1}[2\alpha(\alpha-1)/(1-2\alpha+2\alpha^2)]$ as plotted in Fig. 3.

Therefore, the semi-tangential torque always gives the highest buckling torque at $\beta$=1 as the sharing factor $\alpha$ is fixed at 0.5 in both directions. The quasi-tangential torque always gives the lowest bucking torque at $\beta$=0.5 as the sharing factor $\alpha$ is fixed at 0 in one direction. This is confirmed in the numerical example in Section 11.1 that the buckling torque is 0.78 for quasi-tangential torque, 1.56 for semi-tangential torque and 1.35 for uniform torque when the rigidity ratio $I_x/I_y$=1/1.5. The large discrepancy is not ignorable (Table 1).

Although there are a number of literatures considering torque buckling, e.g., Eick and Migolet [19] on rotating beams, Sinha [20,22] on nonlinear rotation and Paolone et al. [21] on non-conservative buckling, their results cannot be directly compared. As a possible check, we use ANSYS®, a commercial package to analyze the torque buckling of a straight rectangular cantilever beam by means of its beam element (BEAM 189, ANSYS1), solid elements with 4 points loads to simulate the semi-tangential torque (SOLID 45, ANSYS2) and solid elements with distributed loads to simulate the uniform torque (SOLID 45, ANSYS3) for two cases (i) square cross-section $b$=$d$=1 and (ii) rectangular cross-section $b$=1, $d$=2. The buckling load parameters $\lambda=Ll/EI_0$ are tabulated in Tables 2 and 3 for cases (i) and (ii), respectively. It is observed that all computations have similar buckling torque results for square cross-section beams but can be quite different for rectangular cross-section beams. Only results for rectangular cross-section beams need comments. Using existing beam theory, BEAM 189 of ANSYS® produce much lower first buckling torque as expected. ANSYS2 gives lower buckling torque (0.7900) than

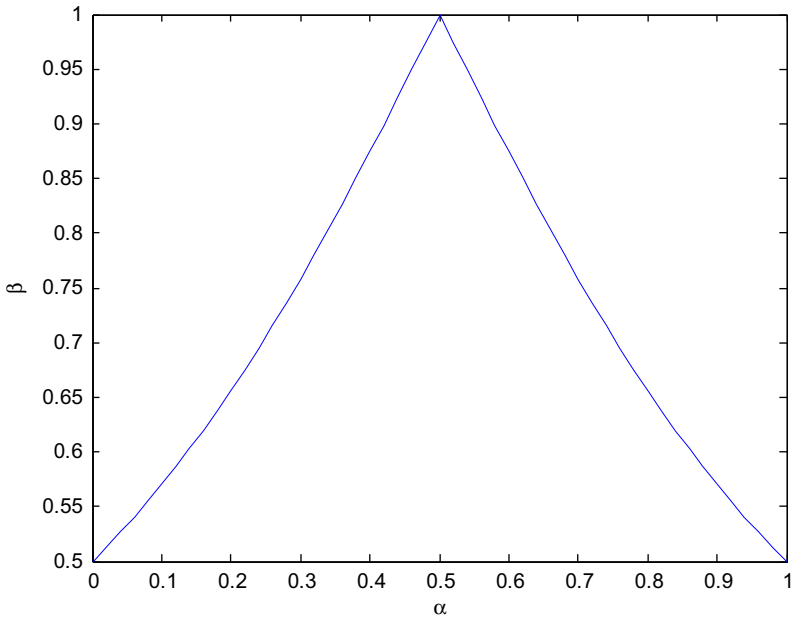


**Fig. 3.** The buckling torque parameter $\beta$ against the sharing factor $\alpha$.

**Table 1**
Comparison of various torque applications.

| | QT1 | QT2 | ST | UT |
|---|---|---|---|---|
| Shear strain $x$ | $\gamma_{zx}^0 = -\frac{yL}{GI_x}$ | $\gamma_{zx}^0 = 0$ | $\gamma_{zx}^0 = -\frac{yL}{2GI_x}$ | $\gamma_{zx}^0 = -\frac{yL}{GJ_0}$ |
| Shear strain $y$ | $\gamma_{zy}^0 = 0$ | $\gamma_{zy}^0 = \frac{xL}{GI_y}$ | $\gamma_{zy}^0 = \frac{xL}{2GI_y}$ | $\gamma_{zy}^0 = \frac{xL}{GJ_0}$ |
| Shear strain arbitrary angle | NA | NA | NA | $\gamma^0 = \frac{rL}{GJ_0}$ |

**Table 2**
Comparing buckling torques for square cross-section beams.

| | **Present**<br>Power series | **ANSYS1**<br>Existing beam theory | **ANSYS2**<br>Torque composed of 4 point loads | **ANSYS3**<br>Torque composed of 121 point loads |
|---|---|---|---|---|
| Element number | 1 | 100 | 10*10*100=10,000 | 10*10*100=10,000 |
| Node number | | 200 | 11*11*101=12,221 | 12,221 |
| DOF | 102 | 1200 | 36,663 | 36,663 |
| **Mode** | | | | |
| 1 | 1.5708 | 1.5708 | 1.5285 | 1.5734 |
| 2 | 1.5708 | 1.5708 | 1.5285 | 1.5734 |
| 3 | 4.7126 | 4.7124 | 4.5873 | 4.7229 |
| 4 | 4.7126 | 4.7124 | 4.5873 | 4.7229 |
| 5 | 7.8548 | 7.854 | 5.5983 | 7.8807 |
| 6 | 7.8548 | 7.854 | 7.6512 | 7.8807 |

the present theory (0.8243) by applying 4 point tangential loads at the free end and ANSYS3 gives higher buckling torque (0.8833) by applying 121 point shear loads distributed over the cross-section at the free end tangential relative to the edge directions and proportional to the distance from the center.

## 3. Strain energy due to initial torque and biaxial moments

We shall apply the classical assumptions of bi-symmetric thin section beams with initial stresses due to biaxial bending moments $M$ along the $x$-axis and $N$ along the $y$-axis, torque $L$ about the $z$-axis, axial force $P$ acting along the centroid $z$-axis which is also the neutral axis and warping moment $B$.

**Table 3**
Comparing buckling torques for rectangular cross-section beams.

| Mode | Present | ANSYS1 Existing beam theory | ANSYS2 Torque composed of 4 point loads | ANSYS3 Torque composed of 121 point loads |
|---|---|---|---|---|
| 1 | 0.8243 | 1.2566 | 0.7900 | 0.8833 |
| 2 | 1.689 | 1.2566 | 1.6219 | 1.5345 |
| 3 | 3.3377 | 3.7699 | 2.9731 | 3.5021 |
| 4 | 4.2024 | 3.7699 | 3.1913 | 4.0538 |
| 5 | 5.8514 | 6.2832 | 4.0418 | 6.0246 |
| 6 | 6.7163 | 6.2832 | 5.5696 | 6.5772 |

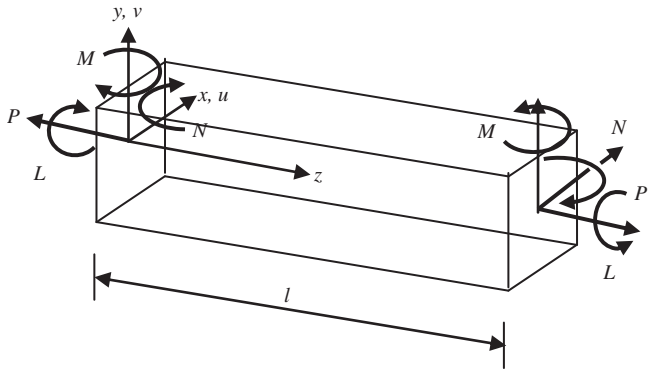


**Fig. 4.** A beam element with initial moments and torque.

The directions of the initial loadings are shown in Fig. 4 in the absence of the warping moment. The initial axial stress is

$$\sigma_z^0 = \frac{P}{A} - \frac{Mx}{I_y} + \frac{Ny}{I_x} + \frac{B\varpi}{I_\varpi} \tag{3}$$

where $\varpi$ is the principal warping coordinate and $I_\varpi = \int \varpi^2 \, dA$ is the principal warping moment of cross-sectional area $A$. The initial stress due to warping moment will be neglected in the subsequent analysis to simplify the presentation. The initial shear stresses due to the uniform torque $L$ are

$$\tau_{zy}^0 = \frac{xL}{J_0} \quad \text{and} \quad \tau_{zx}^0 = -\frac{yL}{J_0} \tag{4}$$

The displacement gradient (1) can be put in vector form

$$\overline{\nabla}\mathbf{u} = \begin{bmatrix} -1 & 0 & 0 & 0 & 0 \\ 0 & 0 & 0 & 0 & 0 \\ 0 & 0 & 1 & 0 & 0 \\ 0 & -1 & 0 & 0 & 0 \\ 0 & 0 & -1 & 0 & 0 \\ 0 & 0 & 0 & 0 & 0 \\ 0 & 0 & 0 & -x & -y \\ 1 & 0 & -y & 0 & 0 \\ 0 & 1 & x & 0 & 0 \end{bmatrix} \begin{Bmatrix} u' \\ v' \\ \theta' \\ u'' \\ v'' \end{Bmatrix} \tag{5}$$

We do not consider axial deformation in a linear buckling analysis for an inextensible column. The strain energy (2) due to the initial stresses can be expressed in matrix form [4]

$$U_\sigma = \frac{1}{2} \int \int (\overline{\nabla}\mathbf{u})^{\mathrm{T}} \begin{bmatrix} \mathbf{0} & \mathbf{0} & \tau_{zx}\mathbf{I} \\ \mathbf{0} & \mathbf{0} & \tau_{zy}\mathbf{I} \\ \tau_{zx}\mathbf{I} & \tau_{zy}\mathbf{I} & \sigma_z\mathbf{I} \end{bmatrix} (\overline{\nabla}\mathbf{u}) \, dA \, dz \tag{6}$$

Substituting Eqs. (3) and (4) into Eq. (6) and integrating over the area, one has

$$U_\sigma = \frac{1}{2}\int \begin{Bmatrix} u' \\ v' \\ \theta' \\ u'' \\ v'' \end{Bmatrix}^{\mathrm{T}} \begin{bmatrix} P & 0 & M & 0 & -\frac{I_x L}{J_0} \\ 0 & P & N & \frac{I_y L}{J_0} & 0 \\ M & N & 0 & 0 & 0 \\ 0 & \frac{I_y L}{J_0} & 0 & 0 & 0 \\ -\frac{I_x L}{J_0} & 0 & 0 & 0 & 0 \end{bmatrix} \begin{Bmatrix} u' \\ v' \\ \theta' \\ u'' \\ v'' \end{Bmatrix} \mathrm{d}z \tag{7}$$

The strain energies due to initial stresses with respect to the quasi-tangential and semi-tangential torques are, respectively,

$$U_{\sigma q} = \frac{1}{2}\int \begin{Bmatrix} u' \\ v' \\ \theta' \\ u'' \\ v'' \end{Bmatrix}^{\mathrm{T}} \begin{bmatrix} P & 0 & M & 0 & 0 \\ 0 & P & N & L & 0 \\ M & N & 0 & 0 & 0 \\ 0 & L & 0 & 0 & 0 \\ 0 & 0 & 0 & 0 & 0 \end{bmatrix} \begin{Bmatrix} u' \\ v' \\ \theta' \\ u'' \\ v'' \end{Bmatrix} \mathrm{d}z \tag{7a}$$

or

$$U_{\sigma q} = \frac{1}{2}\int \begin{Bmatrix} u' \\ v' \\ \theta' \\ u'' \\ v'' \end{Bmatrix}^{\mathrm{T}} \begin{bmatrix} P & 0 & M & 0 & -L \\ 0 & P & N & 0 & 0 \\ M & N & 0 & 0 & 0 \\ 0 & 0 & 0 & 0 & 0 \\ -L & 0 & 0 & 0 & 0 \end{bmatrix} \begin{Bmatrix} u' \\ v' \\ \theta' \\ u'' \\ v'' \end{Bmatrix} \mathrm{d}z \tag{7b}$$

and

$$U_{\sigma s} = \frac{1}{2}\int \begin{Bmatrix} u' \\ v' \\ \theta' \\ u'' \\ v'' \end{Bmatrix}^{\mathrm{T}} \begin{bmatrix} P & 0 & M & 0 & -\frac{1}{2}L \\ 0 & P & N & \frac{1}{2}L & 0 \\ M & N & 0 & 0 & 0 \\ 0 & \frac{1}{2}L & 0 & 0 & 0 \\ -\frac{1}{2}L & 0 & 0 & 0 & 0 \end{bmatrix} \begin{Bmatrix} u' \\ v' \\ \theta' \\ u'' \\ v'' \end{Bmatrix} \mathrm{d}z \tag{7c}$$

## 4. Total potential energy

The principle of stationary total potential energy states that the configuration making the total potential energy a minimum (or stationary) is the equilibrium configuration [4]. The total potential energy $V$ is given by

$$V = U - W \tag{8}$$

where $U$ is the total strain energy and $W$ is the total work done. In our study, the total strain energy is the sum of linear strain energy $U_e$ and the strain energy due to initial stresses $U_\sigma$ of Eq. (7). $U_e$ is given by

$$U_e = \frac{1}{2}\int (GJ\theta'^2 + EI_y u''^2 + EI_x v''^2 + EI_\varpi \theta''^2)\,\mathrm{d}z. \tag{9}$$

where $GJ$ is the torsional rigidity. The total work done due to distributed forces per unit length in the $x$ and $y$ directions $f_x$ and $f_y$ and due to distributed torque per unit length $m_z$, respectively, is

$$W = \int (f_x u + f_y v + m_z \theta)\,\mathrm{d}z \tag{10}$$

If the column is vibration at frequency $\omega$, then the amplitude of work done by inertia forces is

$$W = -\int (\omega^2 \rho A u^2 + \omega^2 \rho A v^2 + \omega^2 \rho J_0 \theta^2)\,\mathrm{d}z$$

$(u, v, \theta)$ are the amplitudes of vibration now. Therefore, the total potential energy is

$$V=\frac{1}{2}\int_0^l \begin{Bmatrix} u\\ v\\ \theta\\ u'\\ v'\\ \theta'\\ u''\\ v''\\ \theta'' \end{Bmatrix}^{\mathrm{T}} \begin{bmatrix} -\omega^2\rho A & 0 & 0 & 0 & 0 & 0 & 0 & 0 & 0\\ 0 & -\omega^2\rho A & 0 & 0 & 0 & 0 & 0 & 0 & 0\\ 0 & 0 & -\omega^2\rho J_0 & 0 & 0 & 0 & 0 & 0 & 0\\ 0 & 0 & 0 & P & 0 & M & 0 & -\frac{I_x L}{J_0} & 0\\ 0 & 0 & 0 & 0 & P & N & \frac{I_y L}{J_0} & 0 & 0\\ 0 & 0 & 0 & M & N & GJ & 0 & 0 & 0\\ 0 & 0 & 0 & 0 & \frac{I_y L}{J_0} & 0 & EI_y & 0 & 0\\ 0 & 0 & 0 & -\frac{I_x L}{J_0} & 0 & 0 & 0 & EI_x & 0\\ 0 & 0 & 0 & 0 & 0 & 0 & 0 & 0 & EI_\varpi \end{bmatrix} \begin{Bmatrix} u\\ v\\ \theta\\ u'\\ v'\\ \theta'\\ u''\\ v''\\ \theta'' \end{Bmatrix} \mathrm{d}z \tag{11}$$

In partitioned matrix form [5], one has

$$V=\frac{1}{2}\int_0^l \begin{Bmatrix} \mathbf{r}\\ \mathbf{r}'\\ \mathbf{r}'' \end{Bmatrix}^{\mathbf{T}} \begin{bmatrix} \mathbf{A}_{00} & \mathbf{A}_{01} & \mathbf{A}_{02}\\ \mathbf{A}_{10} & \mathbf{A}_{11} & \mathbf{A}_{12}\\ \mathbf{A}_{20} & \mathbf{A}_{21} & \mathbf{A}_{22} \end{bmatrix} \begin{Bmatrix} \mathbf{r}\\ \mathbf{r}'\\ \mathbf{r}'' \end{Bmatrix} \mathrm{d}z - \int_0^l \mathbf{R}^{\mathrm{T}}\mathbf{r}\,\mathrm{d}z \tag{12}$$

where

$$\{\mathbf{r}\}=\begin{Bmatrix} u\\ v\\ \theta \end{Bmatrix} \quad \text{and} \quad \mathbf{R}=\begin{Bmatrix} f_x\\ f_y\\ m_z \end{Bmatrix}$$

etc. For equilibrium, $\delta V=0$, where the variation is taken on the unknown displacement $\mathbf{r}$. Therefore,

$$\delta V=\int_0^l \begin{Bmatrix} \mathbf{r}\\ \mathbf{r}'\\ \mathbf{r}'' \end{Bmatrix}^{\mathbf{T}} \begin{bmatrix} \mathbf{A}_{00} & \mathbf{A}_{01} & \mathbf{A}_{02}\\ \mathbf{A}_{10} & \mathbf{A}_{11} & \mathbf{A}_{12}\\ \mathbf{A}_{20} & \mathbf{A}_{21} & \mathbf{A}_{22} \end{bmatrix} \boldsymbol{\delta} \begin{Bmatrix} \mathbf{r}\\ \mathbf{r}'\\ \mathbf{r}'' \end{Bmatrix} \mathrm{d}z - \int_0^l \mathbf{R}^{\mathrm{T}}\,\boldsymbol{\delta}\mathbf{r}\,\mathrm{d}z$$

$$= \int_0^l \begin{Bmatrix} \mathbf{r}\\ \mathbf{r}'\\ \mathbf{r}'' \end{Bmatrix}^{\mathrm{T}} \left( \begin{bmatrix} \mathbf{A}_{00}\\ \mathbf{A}_{10}\\ \mathbf{A}_{20} \end{bmatrix} \boldsymbol{\delta}\mathbf{r} + \begin{bmatrix} \mathbf{A}_{01}\\ \mathbf{A}_{11}\\ \mathbf{A}_{21} \end{bmatrix} \boldsymbol{\delta}\mathbf{r}' + \begin{bmatrix} \mathbf{A}_{02}\\ \mathbf{A}_{12}\\ \mathbf{A}_{22} \end{bmatrix} \boldsymbol{\delta}\mathbf{r}'' \right) \mathrm{d}z - \int_0^l \mathbf{R}^{\mathrm{T}}\,\boldsymbol{\delta}\mathbf{r}\,\mathrm{d}z = 0 \tag{13}$$

We have to replace $\boldsymbol{\delta}\mathbf{r}'$ and $\boldsymbol{\delta}\mathbf{r}''$ by $\boldsymbol{\delta}\mathbf{r}$ using integration by parts, because only $\boldsymbol{\delta}\mathbf{r}$ is independently arbitrary,

$$\int_0^l \begin{Bmatrix} \mathbf{r}\\ \mathbf{r}'\\ \mathbf{r}'' \end{Bmatrix}^{\mathrm{T}} \begin{bmatrix} \mathbf{A}_{01}\\ \mathbf{A}_{11}\\ \mathbf{A}_{21} \end{bmatrix} \boldsymbol{\delta}\mathbf{r}'\,\mathrm{d}z = \int_0^l \begin{Bmatrix} \mathbf{r}\\ \mathbf{r}'\\ \mathbf{r}'' \end{Bmatrix}^{\mathrm{T}} \begin{bmatrix} \mathbf{A}_{01}\\ \mathbf{A}_{11}\\ \mathbf{A}_{21} \end{bmatrix} \mathrm{d}\boldsymbol{\delta}\mathbf{r} = \begin{Bmatrix} \mathbf{r}\\ \mathbf{r}'\\ \mathbf{r}'' \end{Bmatrix}^{\mathrm{T}} \begin{bmatrix} \mathbf{A}_{01}\\ \mathbf{A}_{11}\\ \mathbf{A}_{21} \end{bmatrix} \boldsymbol{\delta}\mathbf{r}|_b - \int_0^l \left( \begin{Bmatrix} \mathbf{r}\\ \mathbf{r}'\\ \mathbf{r}'' \end{Bmatrix}^{\mathrm{T}} \begin{bmatrix} \mathbf{A}_{01}\\ \mathbf{A}_{11}\\ \mathbf{A}_{21} \end{bmatrix} \right)' \boldsymbol{\delta}\mathbf{r}\,\mathrm{d}z$$

$$\int_0^l \begin{Bmatrix} \mathbf{r}\\ \mathbf{r}'\\ \mathbf{r}'' \end{Bmatrix}^{\mathrm{T}} \begin{bmatrix} \mathbf{A}_{02}\\ \mathbf{A}_{12}\\ \mathbf{A}_{22} \end{bmatrix} \boldsymbol{\delta}\mathbf{r}''\,\mathrm{d}z = \begin{Bmatrix} \mathbf{r}\\ \mathbf{r}'\\ \mathbf{r}'' \end{Bmatrix}^{\mathrm{T}} \begin{bmatrix} \mathbf{A}_{02}\\ \mathbf{A}_{12}\\ \mathbf{A}_{22} \end{bmatrix} \boldsymbol{\delta}\mathbf{r}'|_b - \left( \begin{Bmatrix} \mathbf{r}\\ \mathbf{r}'\\ \mathbf{r}'' \end{Bmatrix}^{\mathrm{T}} \begin{bmatrix} \mathbf{A}_{02}\\ \mathbf{A}_{12}\\ \mathbf{A}_{22} \end{bmatrix} \right)' \boldsymbol{\delta}\mathbf{r}|_b + \int_0^l \left( \begin{Bmatrix} \mathbf{r}\\ \mathbf{r}'\\ \mathbf{r}'' \end{Bmatrix}^{\mathrm{T}} \begin{bmatrix} \mathbf{A}_{02}\\ \mathbf{A}_{12}\\ \mathbf{A}_{22} \end{bmatrix} \right)'' \boldsymbol{\delta}\mathbf{r}\,\mathrm{d}z$$

where $|_b$ denotes evaluation at the boundaries. Substituting into Eq. (13), one has

$$\delta V=\int_0^l \left( \begin{Bmatrix} \mathbf{r}\\ \mathbf{r}'\\ \mathbf{r}'' \end{Bmatrix}^{\mathrm{T}} \begin{bmatrix} \mathbf{A}_{00}\\ \mathbf{A}_{10}\\ \mathbf{A}_{20} \end{bmatrix} - \left( \begin{Bmatrix} \mathbf{r}\\ \mathbf{r}'\\ \mathbf{r}'' \end{Bmatrix}^{\mathrm{T}} \begin{bmatrix} \mathbf{A}_{01}\\ \mathbf{A}_{11}\\ \mathbf{A}_{21} \end{bmatrix} \right)' + \left( \begin{Bmatrix} \mathbf{r}\\ \mathbf{r}'\\ \mathbf{r}'' \end{Bmatrix}^{\mathrm{T}} \begin{bmatrix} \mathbf{A}_{02}\\ \mathbf{A}_{12}\\ \mathbf{A}_{22} \end{bmatrix} \right)'' - \mathbf{R}^{\mathrm{T}} \right) \boldsymbol{\delta}\mathbf{r}\,\mathrm{d}z$$
$$+ \left( \begin{Bmatrix} \mathbf{r}\\ \mathbf{r}'\\ \mathbf{r}'' \end{Bmatrix}^{\mathrm{T}} \begin{bmatrix} \mathbf{A}_{01}\\ \mathbf{A}_{11}\\ \mathbf{A}_{21} \end{bmatrix} - \left( \begin{Bmatrix} \mathbf{r}\\ \mathbf{r}'\\ \mathbf{r}'' \end{Bmatrix}^{\mathrm{T}} \begin{bmatrix} \mathbf{A}_{02}\\ \mathbf{A}_{12}\\ \mathbf{A}_{22} \end{bmatrix} \right)' \right) \boldsymbol{\delta}\mathbf{r}|_b + \begin{Bmatrix} \mathbf{r}\\ \mathbf{r}'\\ \mathbf{r}'' \end{Bmatrix}^{\mathrm{T}} \begin{bmatrix} \mathbf{A}_{02}\\ \mathbf{A}_{12}\\ \mathbf{A}_{22} \end{bmatrix} \boldsymbol{\delta}\mathbf{r}'|_b = 0 \tag{14}$$

Since the virtual displacement $\boldsymbol{\delta}\mathbf{r}$ is arbitrary and the right-hand side is constantly zero, the factor in front of $\boldsymbol{\delta}\mathbf{r}$ must be zero to give the governing equation

$$\begin{Bmatrix}\mathbf{r}\\ \mathbf{r}'\\ \mathbf{r}''\end{Bmatrix}^{\mathrm{T}}\begin{bmatrix}\mathbf{A}_{00}\\ \mathbf{A}_{10}\\ \mathbf{A}_{20}\end{bmatrix}-\left(\begin{Bmatrix}\mathbf{r}\\ \mathbf{r}'\\ \mathbf{r}''\end{Bmatrix}^{\mathrm{T}}\begin{bmatrix}\mathbf{A}_{01}\\ \mathbf{A}_{11}\\ \mathbf{A}_{21}\end{bmatrix}\right)'+\left(\begin{Bmatrix}\mathbf{r}\\ \mathbf{r}'\\ \mathbf{r}''\end{Bmatrix}^{\mathrm{T}}\begin{bmatrix}\mathbf{A}_{02}\\ \mathbf{A}_{12}\\ \mathbf{A}_{22}\end{bmatrix}\right)''-\mathbf{R}^{\mathrm{T}}=0 \tag{15}$$

The second line of Eq. (14) must also be zero giving the natural boundary conditions

$$\left(\begin{Bmatrix}\mathbf{r}\\ \mathbf{r}'\\ \mathbf{r}''\end{Bmatrix}^{\mathrm{T}}\begin{bmatrix}\mathbf{A}_{01}\\ \mathbf{A}_{11}\\ \mathbf{A}_{21}\end{bmatrix}-\left(\begin{Bmatrix}\mathbf{r}\\ \mathbf{r}'\\ \mathbf{r}''\end{Bmatrix}^{\mathrm{T}}\begin{bmatrix}\mathbf{A}_{02}\\ \mathbf{A}_{12}\\ \mathbf{A}_{22}\end{bmatrix}\right)'\right)\boldsymbol{\delta}\mathbf{r}|_b+\begin{Bmatrix}\mathbf{r}\\ \mathbf{r}'\\ \mathbf{r}''\end{Bmatrix}^{\mathrm{T}}\begin{bmatrix}\mathbf{A}_{02}\\ \mathbf{A}_{12}\\ \mathbf{A}_{22}\end{bmatrix}\boldsymbol{\delta}\mathbf{r}'|_b=\mathbf{S}_0^{\mathrm{T}}\,\boldsymbol{\delta}\mathbf{r}|_b+\mathbf{S}_1^{\mathrm{T}}\,\boldsymbol{\delta}\mathbf{r}'|_b=0 \tag{16}$$

where $\mathbf{S}_0$ and $\mathbf{S}_1$ are the variationally consistent boundary moments and forces given, respectively, by

$$\mathbf{S}_0^{\mathrm{T}}=\begin{Bmatrix}\mathbf{r}\\ \mathbf{r}'\\ \mathbf{r}''\end{Bmatrix}^{\mathrm{T}}\begin{bmatrix}\mathbf{A}_{01}\\ \mathbf{A}_{11}\\ \mathbf{A}_{21}\end{bmatrix}-\left(\begin{Bmatrix}\mathbf{r}\\ \mathbf{r}'\\ \mathbf{r}''\end{Bmatrix}^{\mathrm{T}}\begin{bmatrix}\mathbf{A}_{02}\\ \mathbf{A}_{12}\\ \mathbf{A}_{22}\end{bmatrix}\right)',\quad \mathbf{S}_1^{\mathrm{T}}=\begin{Bmatrix}\mathbf{r}\\ \mathbf{r}'\\ \mathbf{r}''\end{Bmatrix}^{\mathrm{T}}\begin{bmatrix}\mathbf{A}_{02}\\ \mathbf{A}_{12}\\ \mathbf{A}_{22}\end{bmatrix} \tag{17}$$

Eq. (16) states that, at the boundary, (i) either the displacements are prescribed or the boundary forces are balanced by applied forces and (ii) either the first derivatives of displacements are prescribed or the boundary moments are balanced by applied moments. When the sectional quantities are constant along the length of the column, one has the variationally consistent boundary moments and forces

$$\mathbf{S}_0=[\mathbf{A}_{10}+(\mathbf{A}_{11}-\mathbf{A}_{20})D+(\mathbf{A}_{12}-\mathbf{A}_{21})D^2-\mathbf{A}_{22}D^3]\mathbf{r}\quad\text{and}\quad\mathbf{S}_1=[\mathbf{A}_{20}+\mathbf{A}_{21}D+\mathbf{A}_{22}D^2]\mathbf{r} \tag{18}$$

and the governing equation

$$[\mathbf{A}_{22}D^4-(\mathbf{A}_{12}-\mathbf{A}_{21})D^3+(\mathbf{A}_{20}-\mathbf{A}_{11}+\mathbf{A}_{02})D^2-(\mathbf{A}_{10}-\mathbf{A}_{01})D+\mathbf{A}_{00}]\mathbf{r}=\mathbf{R} \tag{19}$$

in which $D\equiv \mathrm{d}/\mathrm{d}z$.

## 5. Governing equations and natural boundary conditions

Writing in full, the governing equations are

$$\begin{gathered}EI_y u''''+Lv'''-Pu''+M\theta''=f_x-\rho A\omega^2 u,\quad EI_x v''''-Lu'''-Pv''+N\theta''=f_y-\rho A\omega^2 v\\ \text{and}\quad EI_\varpi\theta''''-GJ\theta''+Mu''+Nv''=m_z-\rho J_0\omega^2\theta\end{gathered} \tag{20}$$

and the boundary moments $M_u$, $M_v$, forces $F_u$, $F_v$, torque $M_\theta$ and bimoment $F_\theta$ are

$$M_u=EI_y u''+\frac{I_y L}{J_0}v',\quad F_u=-EI_y u'''+Pu'-Lv''+M\theta' \tag{21}$$

$$M_v=EI_x v''-\frac{I_x L}{J_0}u',\quad F_v=-EI_x v'''+Pv'+Lu''+N\theta' \tag{22}$$

$$M_\theta=EI_\varpi\theta'',\quad F_\theta=-EI_\varpi\theta'''+Mu'+Nv'+GJ\theta' \tag{23}$$

For quasi-tangential torque, the boundary moments should be replaced by either

$$M_u=EI_y u''+Lv'\quad\text{and}\quad M_v=EI_x v''\ \text{or}\ M_u=EI_y u''\quad\text{and}\quad M_v=EI_x v''-Lu' \tag{24}$$

depending on which of the orthogonal direction the torque is applied. These are not defined for any other oblique directions. For semi-tangential torque, the boundary moments should be replaced by

$$M_u=EI_y u''+\tfrac{1}{2}Lv'\quad\text{and}\quad M_v=EI_x v''-\tfrac{1}{2}Lu' \tag{25}$$

Likewise, these are not defined if the fictitious rods are not aligned with the $x$- and $y$-axis. We shall not consider the distributed forces and moment in the subsequent study.

## 6. Solution by power series

Two of the analytical methods in solving Eqs. (20) with the associated boundary conditions are power series and matrix exponent. The matrix exponent method can handle equations of constant coefficients only and the power series is more general. We shall use the power series method here. The power series method has been used extensively to exactly solving a set of governing ordinary linear differential equations with variable coefficients. Eisenberger [6] used power series to obtain the exact dynamics stiffness for non-uniform members.

Leung and coworkers [7–13] published a number of papers on the power series solutions for exact stiffness matrices.

To reduce the number of variable parameters, non-dimensionalization is advantageous. We can always extract one group of parameters out of the integration bracket to eliminate one parameter $EI_y$ say. We can also scale the twist $\theta$, so that either $GJ$ or $EI_\varpi$ can be eliminated. Here, we normalize $EI_\varpi$. Therefore

$$U=\frac{EI_y}{2l^3}\int_0^1 \begin{Bmatrix} u' \\ v' \\ r\theta' \\ u'' \\ v'' \\ r\theta'' \end{Bmatrix}^{\mathrm{T}} \begin{bmatrix} \overline{P} & 0 & \overline{M} & 0 & -e\overline{L} & 0 \\ 0 & \overline{P} & \overline{N} & \overline{L} & 0 & 0 \\ \overline{M} & \overline{N} & K & 0 & 0 & 0 \\ 0 & \overline{L} & 0 & 1 & 0 & 0 \\ -e\overline{L} & 0 & 0 & 0 & e & 0 \\ 0 & 0 & 0 & 0 & 0 & 1 \end{bmatrix} \begin{Bmatrix} u' \\ v' \\ r\theta' \\ u'' \\ v'' \\ r\theta'' \end{Bmatrix} \mathrm{d}\overline{z} \tag{26}$$

where, $\overline{z}=z/l$, $\overline{P}=Pl^2/EI_y$, $\overline{L}=Ll/EJ_0$, $e=EI_x/EI_y$, $r^2=EI_\varpi/EI_y$, $K=GJl^2/(r^2EI_y)=GJl^2/(EI_\varpi)$, $\overline{M}=Ml^2/(rEI_y)$, $\overline{N}=Nl^2/(rEI_y)$, $\overline{\theta}=r\theta$ and a prime denotes differentiation with respect to $\overline{z}$. Dynamic parameters are also required to handle the translational inertia $\overline{w}=\rho A\omega^2 l^4/EI_y$ and the rotational inertia $\overline{g}=J/Ar^2$. We shall drop the over-bars for convenience in the subsequent study. The non-dimensional governing equations are:

$$u''''+(1+e)Lv'''-Pu''-M\theta''=-wu,\quad ev''''-(1+e)Lu'''-Pv''-N\theta''=-wv \quad\text{and}\quad \theta''''-K\theta''-Mu''-Nv''=-gw\theta \tag{27}$$

and the boundary moments and forces are:

$$M_u=u''+Lv',\quad F_u=-u'''+Pu'-(1+e)Lv''+M\theta' \tag{28}$$

$$M_v=ev''-eLu',\quad F_v=-ev'''+Pv'+(1+e)Lu''+N\theta' \tag{29}$$

$$M_\theta=\theta'',\quad F_\theta=-\theta'''+Mu'+Nv'+K\theta' \tag{30}$$

or in vector form

$$\mathbf{M}=\begin{Bmatrix} M_u \\ M_v \\ M_\theta \end{Bmatrix}=\begin{Bmatrix} u''+Lv' \\ ev''-eLu' \\ \theta'' \end{Bmatrix} \quad\text{and}\quad \mathbf{V}=\begin{Bmatrix} F_u \\ F_v \\ F_\theta \end{Bmatrix}=-\begin{Bmatrix} u'''-Pu'+(1+e)Lv''-M\theta' \\ ev'''-Pv'-(1+e)Lu''-N\theta' \\ \theta'''-K\theta'-Mu'-Nv' \end{Bmatrix} \tag{31, 32}$$

Express the solutions in power series

$$\begin{Bmatrix} u(z) \\ v(z) \\ \theta(z) \end{Bmatrix}=\sum_{i=0}^{n}\begin{Bmatrix} u_{k+1} \\ v_{k+1} \\ \theta_{k+1} \end{Bmatrix}z^k \tag{33}$$

Substituting in Eqs. (27) and comparing similar terms in $z^k$, one has

$$u_{k_5}=(wu_{k_1}+Mk_1k_2\theta_{k_3}-(1+e)Lk_1k_2k_3v_{k_1}+Pk_1k_2u_{k_3})/(k_1k_2k_3k_4)$$

$$v_{k_5}=(wv_{k_1}+Nk_1k_2\theta_{k_3}+(1+e)Lk_1k_2k_3u_{k_1}+Pk_1k_2v_{k_3})/(ek_1k_2k_3k_4)$$

$$\theta_{k_5}=(gw\theta_{k_1}+Kk_1k_2\theta_{k_3}+Mk_1k_2k_3u_{k_1}+Nk_1k_2v_{k_3})/(k_1k_2k_3k_4)$$

where

$$k_i=k+i \tag{34}$$

It is obvious that $u_k, v_k, \theta_k$, $k>4$, can be expressed in terms of the 12 integration constants $u_1,u_2,u_3,u_4$; $v_1,v_2,v_3,v_4$; $\theta_1,\theta_2,\theta_3,\theta_4$ for the three ordinary differential equations of order four. Back substituting into Eq. (27), it can be seen that the residue decays rapidly. The slowest term converges about $(4+k)$ times the previous one. When $k$ is about 10, each increment increases the number of significant digit by one. Therefore, 50 terms should achieve more than machine precision in all cases. In case that some coefficients are much bigger than the others, more terms are required. One efficient way to check the convergence of the series solution is by checking the symmetry of the resulting stiffness matrix discussed later.

The power series displacement solutions can be written as

$$\mathbf{r}(z)=\begin{Bmatrix} u(z) \\ v(z) \\ \theta(z) \end{Bmatrix}=[\boldsymbol{\chi}_1(z)\ \boldsymbol{\chi}_2(z)\ \ldots\ \boldsymbol{\chi}_{12}(z)][u_1\ \ldots\ \theta_4]^{\mathrm{T}}=\boldsymbol{\chi}(z)\mathbf{c} \tag{35}$$

**Table 4**
The coefficient of the displacement functions.

| | $z^9$ | $z^8$ | $z^7$ | $z^6$ | $z^5$ | $z^4$ | $z^3$ | $z^2$ | $z^1$ | $z^0$ |
|---|---|---|---|---|---|---|---|---|---|---|
| $\chi_u^T=\sum_{i=0}^{9}\chi_{ui}^T z^i$ | 0 | 0.0008 | 0 | −0.0072 | 0 | 0.0417 | 0 | 0 | 0 | 1.0000 |
| | 0.0001 | 0 | −0.0010 | 0 | 0.0083 | 0 | 0 | 0 | 1.0000 | 0 |
| | −0.0017 | 0.0075 | −0.0007 | 0.0199 | 0 | −0.0833 | 0 | 1.0000 | 0 | 0 |
| | −0.0000 | −0.0000 | 0.0375 | 0 | −0.2583 | 0 | 1.0000 | 0 | 0 | 0 |
| | −0.0002 | 0.0000 | 0.0019 | 0 | −0.0139 | 0 | 0 | 0 | 0 | 0 |
| | 0.0000 | 0.0002 | 0 | −0.0023 | 0 | 0 | 0 | 0 | 0 | 0 |
| | −0.0013 | 0.0092 | −0.0052 | 0.0028 | 0.0278 | 0 | 0 | 0 | 0 | 0 |
| | 0.0031 | −0.0137 | 0.0012 | 0.1215 | 0 | −0.6250 | 0 | 0 | 0 | 0 |
| | −0.0246 | 0.1335 | −0.0095 | 0.0400 | 0 | 0 | 0 | 0 | 0 | 0 |
| | 0.0148 | −0.0012 | 0.0057 | 0 | 0 | 0 | 0 | 0 | 0 | 0 |
| | −0.3289 | 1.7824 | −0.1231 | 0.5190 | −0.0278 | 0.0833 | 0 | 0 | 0 | 0 |
| | 0.5941 | −0.0462 | 0.2224 | −0.0139 | 0.0500 | 0 | 0 | 0 | 0 | 0 |
| $\chi_v^T=\sum_{i=0}^{9}\chi_{vi}^T z^i$ | 0.0002 | 0.0000 | −0.0019 | 0 | 0.0139 | 0 | 0 | 0 | 0 | 0 |
| | 0.0000 | −0.0002 | 0 | 0.0023 | 0 | 0 | 0 | 0 | 0 | 0 |
| | 0.0013 | 0.0062 | 0.0052 | 0.0019 | −0.0278 | 0 | 0 | 0 | 0 | 0 |
| | 0.0021 | 0.0091 | 0.0008 | −0.0810 | 0 | 0.4167 | 0 | 0 | 0 | 0 |
| | −0.0000 | 0.0005 | 0 | −0.0045 | 0 | 0.0278 | 0 | 0 | 0 | 1.0000 |
| | 0.0001 | 0 | −0.0006 | 0 | 0.0056 | 0 | 0 | 0 | 1.0000 | 0 |
| | 0.0017 | 0.0051 | 0.0007 | 0.0127 | 0 | −0.0556 | 0 | 1.0000 | 0 | 0 |
| | −0.0008 | 0.0000 | 0.0344 | 0 | −0.2417 | 0 | 1.0000 | 0 | 0 | 0 |
| | 0.0246 | 0.0891 | 0.0095 | 0.0267 | 0 | 0 | 0 | 0 | 0 | 0 |
| | 0.0099 | 0.0012 | 0.0038 | 0 | 0 | 0 | 0 | 0 | 0 | 0 |
| | 0.3289 | 1.1903 | 0.1231 | 0.3466 | 0.0278 | 0.0556 | 0 | 0 | 0 | 0 |
| | 0.3968 | 0.0462 | 0.1485 | 0.0139 | 0.0333 | 0 | 0 | 0 | 0 | 0 |
| $\chi_\theta^T=\sum_{i=0}^{9}\chi_{\theta i}^T z^i$ | 0.0009 | 0.0046 | 0.0003 | 0.0014 | 0 | 0 | 0 | 0 | 0 | 0 |
| | 0.0005 | 0.0000 | 0.0002 | 0 | 0 | 0 | 0 | 0 | 0 | 0 |
| | −0.0017 | 1.8209 | −0.0007 | 0.5306 | 0 | 0.0833 | 0 | 0 | 0 | 0 |
| | 0.5941 | 0.0462 | 0.2224 | 0.0139 | 0.0500 | 0 | 0 | 0 | 0 | 0 |
| | −0.0009 | 0.0031 | −0.0003 | 0.0009 | 0 | 0 | 0 | 0 | 0 | 0 |
| | 0.0003 | −0.0000 | 0.0001 | 0 | 0 | 0 | 0 | 0 | 0 | 0 |
| | 0.0017 | 1.8239 | 0.0007 | 0.5315 | 0 | 0.0833 | 0 | 0 | 0 | 0 |
| | 0.5951 | −0.0693 | 0.2228 | −0.0208 | 0.0500 | 0 | 0 | 0 | 0 | 0 |
| | 0 | 26.3532 | 0 | 7.6800 | 0 | 1.2000 | 0 | 0 | 0 | 1.0000 |
| | 2.9281 | 0 | 1.0971 | 0 | 0.2400 | 0 | 0 | 0 | 1.0000 | 0 |
| | 0 | 351.6656 | 0 | 102.4846 | 0 | 16.0000 | 0 | 1.0000 | 0 | 0 |
| | 117.2219 | 0 | 43.9220 | 0 | 9.6000 | 0 | 1.0000 | 0 | 0 | 0 |

in which

$$\boldsymbol{\chi}(z)=\begin{Bmatrix}\boldsymbol{\chi}_u(z)\\ \boldsymbol{\chi}_v(z)\\ \boldsymbol{\chi}_\theta(z)\end{Bmatrix}$$

is a $3\times 12$ matrix of the computed displacement shape functions given by Eqs. (34) and vector $\mathbf{c}$ contains the integration constants to be determined by the prescribed nodal displacements. The first few terms of matrix $\boldsymbol{\chi}(z)$ are actually identity matrix corresponding to the integration constants. The explicit form of the displacement functions are listed in Table 4 in the numerical example section. To get the shape functions from the displacement functions (35), the following displacement boundary conditions evaluated at $z=0$ and $z=1$ are required for the nodal displacement vector $\mathbf{q}$,

$$\mathbf{q}^T=[u(0)\ \ v(0)\ \ \theta(0)\ \ u'(0)\ \ v'(0)\ \ \theta'(0)\ \ u(1)\ \ v(1)\ \ \theta(1)\ \ u'(1)\ \ v'(1)\ \ \theta'(1)]$$

$$\mathbf{q}=\begin{bmatrix}\boldsymbol{\chi}(0)\\ \boldsymbol{\chi}'(0)\\ \boldsymbol{\chi}(1)\\ \boldsymbol{\chi}'(1)\end{bmatrix}\mathbf{c}=\mathbf{C}\mathbf{c}\quad\text{for}\quad\mathbf{C}=\begin{bmatrix}\boldsymbol{\chi}(0)\\ \boldsymbol{\chi}'(0)\\ \boldsymbol{\chi}(1)\\ \boldsymbol{\chi}'(1)\end{bmatrix}\ \text{or}\ \mathbf{c}=\mathbf{C}^{-1}\mathbf{q}$$

and the shape functions $\mathbf{N}$ are given by

$$\mathbf{r}(z)=\begin{Bmatrix}u(z)\\ v(z)\\ \theta(z)\end{Bmatrix}=\boldsymbol{\chi}(z)\mathbf{c}=\boldsymbol{\chi}(z)\mathbf{C}^{-1}\mathbf{q}=\mathbf{N}(z)\mathbf{q}\tag{36}$$

where $\mathbf{N}(z)=\boldsymbol{\chi}(z)\mathbf{C}^{-1}$ is the shape function matrix in the finite element sense. The exact stiffness matrix $\mathbf{K}$ is given by substituting Eq. (36) into (31, 32) and evaluating the boundary forces and moments from Eqs. (31, 32)

$$\mathbf{F}=\begin{Bmatrix}-\mathbf{V}(0)\\-\mathbf{M}(0)\\\mathbf{V}(1)\\\mathbf{M}(1)\end{Bmatrix}=\mathbf{K}\mathbf{q} \tag{37}$$

The negative signs are in consistence with the negative end of the column. It can be shown that the stiffness matrix thus obtained is symmetrical to fulfill the requirement of the reciprocal theorem. The symmetry is an efficient check on the convergence of the power series solution in the number of polynomial terms taken. The number of terms should be increased if the final matrix is not symmetrical. Eq. (37) is the final stiffness equation that can be connected to the stiffness matrices of other structures using the conditions of equilibrium and compatibility at joints to form the global stiffness matrix.

## 7. Non-uniformity

When the cross-sectional area or any of the loadings is non-uniform, one has to solve the non-uniform set of equations (15) with the associated natural boundary conditions (17). Writing in full, one has

$$\mathbf{A}_{00}\mathbf{r}+\mathbf{A}_{01}\mathbf{r}'+\mathbf{A}_{02}\mathbf{r}''-(\mathbf{A}_{10}\mathbf{r})'-(\mathbf{A}_{11}\mathbf{r}')'-(\mathbf{A}_{12}\mathbf{r}'')'+(\mathbf{A}_{20}\mathbf{r})''+(\mathbf{A}_{21}\mathbf{r}')''+(\mathbf{A}_{22}\mathbf{r}'')''=\mathbf{R} \tag{43}$$

$$\mathbf{S}_0=\mathbf{A}_{10}\mathbf{r}+\mathbf{A}_{11}\mathbf{r}'+\mathbf{A}_{12}\mathbf{r}''-(\mathbf{A}_{20}\mathbf{r})'-(\mathbf{A}_{21}\mathbf{r}')'-(\mathbf{A}_{22}\mathbf{r}'')' \tag{44}$$

$$\mathbf{S}_1=\mathbf{A}_{20}\mathbf{r}+\mathbf{A}_{21}\mathbf{r}'+\mathbf{A}_{22}\mathbf{r}'' \tag{45}$$

To study the convergence of the power series method for non-uniform beam, let us consider a much simpler problem in the absence of all secondary loads whose governing equation is

$$(ev'')''-wv=0 \tag{46}$$

where $w=\omega^2\rho Al^4/EI$, $\omega$ is the frequency, $\rho A$ is mass per unit length, $EI$ is the nominal flexural rigidity and $e=(1+fz)^3$ to study the effect of non-uniformity due to linear varying depth. The power series solution is

$$v_{k+5}=\frac{wv_{k+1}-f^3k(1+k)^2(2+k)v_{k+2}-3f^2(1+k)^2(2+k)^2v_{k+3}-3f(1+k)(2+k)^2(3+k)v_{k+4}}{(1+k)(2+k)(3+k)(4+k)} \tag{47}$$

That the numerator and denominator equally contain $k$ to the power four poses a serious convergent problem. Back-substitute into Eq. (46) using 10 terms, the output residue is excessively large and convergence cannot be guaranteed.

## 8. Extended Leung's theorem

It is evident that the stiffness matrix $\mathbf{K}$ is nonlinearly dependent on the loading parameters $(P,L,M,N)$ and exact solution methods are not available. For some versions of Newtonian iteration to be discussed later, the partial derivatives of the stiffness matrix with respect to these parameters are required. It is seen from Eqs. (36) and (37) that the analytic dynamic stiffness matrix is formed from several matrix products involving matrix inversion; direct matrix derivatives will be very difficult.

A simple matrix differentiation of the dynamic stiffness can be obtained by using the fact that the exact stiffness is the condensed finite element matrix after all the internal nodal displacements are accurately eliminated. Let $\mathbf{q}_2$ be the external nodal displacements at the two outer most nodes and $\mathbf{q}_1$ be all the external nodal displacements to be eliminated so that $\mathbf{q}=\begin{Bmatrix}\mathbf{q}_1\\\mathbf{q}_2\end{Bmatrix}$. Consider just one second-order loading parameter, $\lambda$, say, the finite element equation is

$$\mathbf{K}(\lambda)\mathbf{q}=[\mathbf{A}+\lambda\mathbf{B}]\mathbf{q}=\mathbf{f} \tag{48}$$

where $\mathbf{f}$ is the first-order nodal forces. Assuming that the first-order nodal force applies to the outer most nodes only, Eq. (48) can be partitioned as

$$\begin{bmatrix}\mathbf{K}_{11}&\mathbf{K}_{12}\\\mathbf{K}_{21}&\mathbf{K}_{22}\end{bmatrix}\begin{Bmatrix}\mathbf{q}_1\\\mathbf{q}_2\end{Bmatrix}=\left(\begin{bmatrix}\mathbf{A}_{11}&\mathbf{A}_{12}\\\mathbf{A}_{21}&\mathbf{A}_{22}\end{bmatrix}+\lambda\begin{bmatrix}\mathbf{B}_{11}&\mathbf{B}_{12}\\\mathbf{B}_{21}&\mathbf{B}_{22}\end{bmatrix}\right)\begin{Bmatrix}\mathbf{q}_1\\\mathbf{q}_2\end{Bmatrix}=\begin{Bmatrix}0\\\mathbf{f}_2\end{Bmatrix} \tag{49}$$

for constant matrices $\mathbf{A}_{ij}$ and $\mathbf{B}_{ij}$. From Eq. (48), one has the transformation,

$$\mathbf{q}=\begin{bmatrix}-\mathbf{K}_{11}^{-1}\mathbf{K}_{12}\\\mathbf{I}\end{bmatrix}\mathbf{q}_2=\mathbf{T}(\lambda)\mathbf{q}_2 \tag{50}$$

Eq. (48) becomes, after post-multiplying by $\mathbf{T}^{\mathrm{T}}(\lambda)$,

$$\mathbf{T}^{\mathrm{T}}\mathbf{K}\mathbf{T}\mathbf{q}_2=[\mathbf{T}^{\mathrm{T}}\mathbf{A}\mathbf{T}+\lambda\mathbf{T}^{\mathrm{T}}\mathbf{B}\mathbf{T}]\mathbf{q}_2=\mathbf{f}_2 \tag{51}$$

or

$$\tilde{\mathbf{K}}(\lambda)\mathbf{q}_2=[\tilde{\mathbf{A}}(\lambda)+\lambda\tilde{\mathbf{B}}(\lambda)]\mathbf{q}_2=\mathbf{f}_2 \tag{52}$$

where $\tilde{\mathbf{K}},\tilde{\mathbf{A}},\tilde{\mathbf{B}}$ are the condensed matrices. If sufficient number of finite elements is taken, the condensed matrices become the exact matrices being studied. We are required to prove the Leung theorem [14,15] that

$$\tilde{\mathbf{K}}'(\lambda)=\frac{\partial\tilde{\mathbf{K}}(\lambda)}{\partial\lambda}=\tilde{\mathbf{B}}(\lambda) \tag{53}$$

The derivative of the transformation matrix is

$$\mathbf{T}'(\lambda)=\frac{\partial}{\partial\lambda}\mathbf{T}(\lambda)=\frac{\partial}{\partial\lambda}\begin{bmatrix}-\mathbf{K}_{11}^{-1}\mathbf{K}_{12}\\ \mathbf{I}\end{bmatrix}=\begin{bmatrix}\mathbf{K}_{11}^{-1}\mathbf{B}_{11}\mathbf{K}_{11}^{-1}\mathbf{K}_{12}-\mathbf{K}_{11}^{-1}\mathbf{B}_{12}\\ \mathbf{0}\end{bmatrix} \tag{54}$$

where the derivative of $\mathbf{K}_{11}^{-1}$ has been obtained using the fact that

$$\mathbf{K}_{11}^{-1}\mathbf{K}_{11}=\mathbf{I},\quad (\mathbf{K}_{11}^{-1})'\mathbf{K}_{11}+\mathbf{K}_{11}^{-1}\mathbf{K}_{11}'=\mathbf{0}\quad\text{and}\quad(\mathbf{K}_{11}^{-1})'=-\mathbf{K}_{11}^{-1}\mathbf{K}_{11}'\,\mathbf{K}_{11}^{-1}=-\mathbf{K}_{11}^{-1}\mathbf{B}_{11}\mathbf{K}_{11}^{-1}$$

Therefore,

$$\tilde{\mathbf{K}}'(\lambda)=\frac{\partial\tilde{\mathbf{K}}(\lambda)}{\partial\lambda}=\mathbf{T}'\mathrm{T}\mathbf{K}\mathbf{T}+\mathbf{T}^{\mathrm{T}}\mathbf{K}'\mathbf{T}+\mathbf{T}^{\mathrm{T}}\mathbf{K}\mathbf{T}'=\mathbf{T}^{\mathrm{T}}\mathbf{B}\mathbf{T}=\tilde{\mathbf{B}}(\lambda)$$

as required because $\mathbf{T}'\mathrm{T}\mathbf{K}\mathbf{T}=\mathbf{0}$ and $\mathbf{T}^{\mathrm{T}}\mathbf{K}\mathbf{T}'=\mathbf{0}$ from Eq. (54). An alternative proof is that

$$\tilde{\mathbf{K}}=\mathbf{K}_{22}-\mathbf{K}_{21}\mathbf{K}_{11}^{-1}\mathbf{K}_{12}=\begin{bmatrix}-\mathbf{K}_{11}^{-1}\mathbf{K}_{12}\\ \mathbf{I}\end{bmatrix}^{\mathrm{T}}\begin{bmatrix}\mathbf{K}_{11} & \mathbf{K}_{12}\\ \mathbf{K}_{21} & \mathbf{K}_{22}\end{bmatrix}\begin{bmatrix}-\mathbf{K}_{11}^{-1}\mathbf{K}_{12}\\ \mathbf{I}\end{bmatrix} \tag{55}$$

and

$$\begin{aligned}\tilde{\mathbf{K}}'=\mathbf{K}_{22}'-\mathbf{K}_{21}'\,\mathbf{K}_{11}^{-1}\mathbf{K}_{12}-\mathbf{K}_{21}\mathbf{K}_{11}^{-1}\mathbf{K}_{12}'+\mathbf{K}_{21}\mathbf{K}_{11}^{-1}\mathbf{K}_{11}'\,\mathbf{K}_{11}^{-1}\mathbf{K}_{12}&=\begin{bmatrix}-\mathbf{K}_{11}^{-1}\mathbf{K}_{12}\\ \mathbf{I}\end{bmatrix}^{\mathrm{T}}\begin{bmatrix}\mathbf{K}_{11}' & \mathbf{K}_{12}'\\ \mathbf{K}_{21}' & \mathbf{K}_{22}'\end{bmatrix}\begin{bmatrix}-\mathbf{K}_{11}^{-1}\mathbf{K}_{12}\\ \mathbf{I}\end{bmatrix}\\ &=\begin{bmatrix}-\mathbf{K}_{11}^{-1}\mathbf{K}_{12}\\ \mathbf{I}\end{bmatrix}^{\mathrm{T}}\begin{bmatrix}\mathbf{B}_{11} & \mathbf{B}_{12}\\ \mathbf{B}_{21} & \mathbf{B}_{22}\end{bmatrix}\begin{bmatrix}-\mathbf{K}_{11}^{-1}\mathbf{K}_{12}\\ \mathbf{I}\end{bmatrix}=\tilde{\mathbf{B}}\end{aligned} \tag{56}$$

which is as stated in Eq. (53).

## 9. Derivatives of the dynamic stiffness matrix

The total strain energy is

$$\begin{aligned}U&=\frac{EI_y}{2l^3}\int_0^1\begin{Bmatrix}u'\\ v'\\ \theta'\\ u''\\ v''\\ \theta''\end{Bmatrix}^{\mathrm{T}}\begin{bmatrix}P & 0 & M & 0 & -eL & 0\\ 0 & P & N & L & 0 & 0\\ M & N & K & 0 & 0 & 0\\ 0 & L & 0 & 1 & 0 & 0\\ -eL & 0 & 0 & 0 & e & 0\\ 0 & 0 & 0 & 0 & 0 & 1\end{bmatrix}\begin{Bmatrix}u'\\ v'\\ \theta'\\ u''\\ v''\\ \theta''\end{Bmatrix}\mathrm{d}z\\ &=\frac{EI_y}{2l^3}\mathbf{q}^{\mathrm{T}}\int_0^1\begin{bmatrix}\mathbf{N}''(z)\\ \mathbf{N}''(z)\end{bmatrix}^{\mathrm{T}}\begin{bmatrix}P & 0 & M & 0 & -eL & 0\\ 0 & P & N & L & 0 & 0\\ M & N & K & 0 & 0 & 0\\ 0 & L & 0 & 1 & 0 & 0\\ -eL & 0 & 0 & 0 & e & 0\\ 0 & 0 & 0 & 0 & 0 & 1\end{bmatrix}\begin{bmatrix}\mathbf{N}''(z)\\ \mathbf{N}''(z)\end{bmatrix}\mathrm{d}z\mathbf{q}\end{aligned} \tag{57}$$

Therefore,

$$\frac{\partial \mathbf{K}}{\partial P} = \mathbf{K}_{,P} = \frac{EI_y}{2l^3}\int_0^1 \begin{bmatrix} \mathbf{N}''(z) \\ \mathbf{N}''(z) \end{bmatrix}^{\mathrm{T}} \begin{bmatrix} 1 & 0 & 0 & 0 & 0 & 0 \\ 0 & 1 & 0 & 0 & 0 & 0 \\ 0 & 0 & 0 & 0 & 0 & 0 \\ 0 & 0 & 0 & 0 & 0 & 0 \\ 0 & 0 & 0 & 0 & 0 & 0 \\ 0 & 0 & 0 & 0 & 0 & 0 \end{bmatrix} \begin{bmatrix} \mathbf{N}''(z) \\ \mathbf{N}''(z) \end{bmatrix} \mathrm{d}z = \frac{EI_y}{2l^3}\mathbf{C}^{-\mathrm{T}} \int_0^1 (\boldsymbol{\chi}_u'^{\mathrm{T}}\boldsymbol{\chi}_u' + \boldsymbol{\chi}_v'^{\mathrm{T}}\boldsymbol{\chi}_v')\,\mathrm{d}z\mathbf{C}^{-1} \tag{58}$$

$$\frac{\partial \mathbf{K}}{\partial L} = \mathbf{K}_{,L} = \frac{EI_y}{2l^3}\int_0^1 \begin{bmatrix} \mathbf{N}'(z) \\ \mathbf{N}''(z) \end{bmatrix}^{\mathrm{T}} \begin{bmatrix} 0 & 0 & 0 & 0 & -e & 0 \\ 0 & 0 & 0 & 1 & 0 & 0 \\ 0 & 0 & 0 & 0 & 0 & 0 \\ 0 & 1 & 0 & 0 & 0 & 0 \\ -e & 0 & 0 & 0 & 0 & 0 \\ 0 & 0 & 0 & 0 & 0 & 0 \end{bmatrix} \begin{bmatrix} \mathbf{N}'(z) \\ \mathbf{N}''(z) \end{bmatrix} \mathrm{d}z = \frac{EI_y}{2l^3}\mathbf{C}^{-T} \int_0^1 (\boldsymbol{\chi}_u''^{\mathrm{T}}\boldsymbol{\chi}_v' + \boldsymbol{\chi}_v'^{\mathrm{T}}\boldsymbol{\chi}_u'' - e\boldsymbol{\chi}_v''^{\mathrm{T}}\boldsymbol{\chi}_u' - e\boldsymbol{\chi}_u'^{\mathrm{T}}\boldsymbol{\chi}_v'')\,\mathrm{d}z\mathbf{C}^{-1} \tag{59}$$

$$\frac{\partial \mathbf{K}}{\partial M} = \mathbf{K}_{,M} = \frac{EI_y}{2l^3}\int_0^l \begin{bmatrix} \mathbf{N}'(z) \\ \mathbf{N}''(z) \end{bmatrix}^{\mathrm{T}} \begin{bmatrix} 0 & 0 & 1 & 0 & 0 & 0 \\ 0 & 0 & 0 & 0 & 0 & 0 \\ 1 & 0 & 0 & 0 & 0 & 0 \\ 0 & 0 & 0 & 0 & 0 & 0 \\ 0 & 0 & 0 & 0 & 0 & 0 \\ 0 & 0 & 0 & 0 & 0 & 0 \end{bmatrix} \begin{bmatrix} \mathbf{N}'(z) \\ \mathbf{N}''(z) \end{bmatrix} \mathrm{d}z = \frac{EI_y}{2l^3}\mathbf{C}^{-\mathrm{T}} \int_0^1 (\boldsymbol{\chi}_u'^{\mathrm{T}}\boldsymbol{\chi}_\theta'^{\mathrm{T}} \mp \boldsymbol{\chi}_\theta \quad \boldsymbol{\chi}_u')\,\mathrm{d}z\mathbf{C}^{-1} \tag{60}$$

$$\frac{\partial \mathbf{K}}{\partial N} = \mathbf{K}_{,N} = \frac{EI_y}{2l^3}\int_0^l \begin{bmatrix} \mathbf{N}'(z) \\ \mathbf{N}''(z) \end{bmatrix}^{\mathrm{T}} \begin{bmatrix} 0 & 0 & 0 & 0 & 0 & 0 \\ 0 & 0 & 1 & 0 & 0 & 0 \\ 0 & 1 & 0 & 0 & 0 & 0 \\ 0 & 0 & 0 & 0 & 0 & 0 \\ 0 & 0 & 0 & 0 & 0 & 0 \\ 0 & 0 & 0 & 0 & 0 & 0 \end{bmatrix} \begin{bmatrix} \mathbf{N}'(z) \\ \mathbf{N}''(z) \end{bmatrix} \mathrm{d}z = \frac{EI_y}{2l^3}\mathbf{C}^{-\mathrm{T}} \int_0^1 (\boldsymbol{\chi}_v'^{\mathrm{T}}\boldsymbol{\chi}_u'^{\theta} + \boldsymbol{\chi}'\mathrm{T}_\theta\boldsymbol{\chi}_v')\,\mathrm{d}z\mathbf{C}^{-1} \tag{61}$$

$$\frac{\partial \mathbf{K}}{\partial w} = \mathbf{K}_{,w} = -\frac{EI_y}{2l^3}\int_0^1 \mathbf{N}(z)^{\mathrm{T}} \begin{bmatrix} 1 & 0 & 0 \\ 0 & 1 & 0 \\ 0 & 0 & g \end{bmatrix} \mathbf{N}(z)\,\mathrm{d}z - \frac{EI_y}{2l^3}\mathbf{C}^{-\mathrm{T}} \int_0^1 (\boldsymbol{\chi}_u^{\mathrm{T}}\boldsymbol{\chi}_u + \boldsymbol{\chi}_v^{\mathrm{T}}\boldsymbol{\chi}_v + \boldsymbol{\chi}_\theta^{\mathrm{T}}\boldsymbol{\chi}_\theta)\,\mathrm{d}z\mathbf{C}^{-1}$$

where the shape function $\mathbf{N}(z)$ is given explicitly by Eq. (36) and $\boldsymbol{\chi}$ in (35).

## 10. Solution of the eigenvalue problem

The equation to be solved in a dynamic buckling problem is

$$\mathbf{K}(\omega^2, P, L, M, N)\mathbf{q} = 0 \tag{62}$$

For non-trivial solution, $\mathbf{q} \neq 0$ and $\det \mathbf{K}(\omega^2, P, L, M, N) = 0$ gives a relation between $(\omega^2, P, L, M, N)$ when buckling occurs. If the order of $\mathbf{K}$ is large, parametric study is difficult. The inverse iteration method generalized below is an alternative efficient method for multi-parameter study.

Assuming an initial approximation is found so that

$$\mathbf{K}_0(\omega_0^2, P_0, L_0, M_0, N_0)\mathbf{q}_0 = 0 \tag{63}$$

with the normalization condition $\mathbf{q}_0^{\mathrm{T}}\mathbf{q}_0 = 1$. After small parametric increment, a new eigenvalue problem to be solved is

$$(\mathbf{K}_0 + \Delta\mathbf{K})(\mathbf{q}_0 + \Delta\mathbf{q}) = 0 \tag{64}$$

where $\Delta\mathbf{K} = \mathbf{K}_{,\omega^2}\,\Delta\omega^2 + \mathbf{K}_{,P}\,\Delta P + \mathbf{K}_{,L}\,\Delta L + \mathbf{K}_{,M}\,\Delta M + \mathbf{K}_{,N}\,\Delta N$ Let us consider the increment of $P$ only. Eq. (64) gives

$$[\mathbf{K}_0 + \Delta P\,\mathbf{K}_{,P}]\{\mathbf{q}_0 + \Delta\mathbf{q}\} = [\mathbf{K}_0 + \Delta P\,\mathbf{K}_{,P}]\mathbf{q}_0 + [\mathbf{K}_0 + \Delta P\,\mathbf{K}_{,P}]\Delta\mathbf{q} = 0 \tag{65}$$

Since $\mathbf{K}_0\mathbf{q}_0 = 0$, therefore $\Delta P[\mathbf{K}_{,P}]\mathbf{q}_0 + [\mathbf{K}_0 + \Delta P\,\mathbf{K}_{,P}]\Delta\mathbf{q} = 0$, or

$$[\mathbf{K}_0 + \Delta P\,\mathbf{K}_{,P}]\Delta\mathbf{q} = -\Delta P[\mathbf{K}_{,P}]\mathbf{q}_0 \tag{66}$$

This is the inverse iteration scheme. The improved eigenvector is given by $\mathbf{q}=\mathbf{q}_0+\Delta\mathbf{q}$ and the improved increment is given by the generalized Rayleigh's quotient

$$\overline{\Delta}P=\frac{\mathbf{q}^{\mathrm{T}}[\mathbf{K}_0+\Delta P\,\mathbf{K}_{,P}]\mathbf{q}}{\mathbf{q}^{\mathrm{T}}[\mathbf{K}_{,P}]\mathbf{q}} \tag{67}$$

Alternatively, one can make arbitrarily small increments on $(\omega^2,P,L,M)$ but not on $N$ so that $\Delta N=0$ in the beginning and find the necessary increment on $N$ to satisfy the eigenvalue problem. Since $\mathbf{K}_0\mathbf{q}_0=0$, Eq. (64) gives

$$(\mathbf{K}_0+\Delta\mathbf{K})(\mathbf{q}_0+\Delta\mathbf{q})=\Delta\mathbf{K}\mathbf{q}_0+(\mathbf{K}_0+\Delta\mathbf{K})\Delta\mathbf{q}=0 \tag{68}$$

$$(\mathbf{K}_0+\Delta\mathbf{K})\Delta\mathbf{q}=-\Delta\mathbf{K}\mathbf{q}_0 \tag{69}$$

Adding $(\mathbf{K}_0+\Delta\mathbf{K})\mathbf{q}_0$ on both sides, one has

$$(\mathbf{K}_0+\Delta\mathbf{K})(\mathbf{q}_0+\Delta\mathbf{q})=\mathbf{K}_0\mathbf{q}_0 \tag{70}$$

This is the inverse iteration scheme for $\mathbf{q}=\mathbf{q}_0+\Delta\mathbf{q}$. The increment $\Delta N$ is then found from the Rayleigh quotient

$$\Delta N=\frac{\mathbf{q}^{\mathrm{T}}(\mathbf{K}_0+\Delta\mathbf{K})\mathbf{q}}{\mathbf{q}^{\mathrm{T}}(\mathbf{K}_{,N})\mathbf{q}} \tag{71}$$

Using either scheme, one can draw the interactive buckling curve or surface in a multi-parametric space. For cluster modes, the subspace iteration [17,18] should be used.

## 11. Numerical examples

Consider a column having rectangular thin walled section as shown in Fig. 5.

The dimensions are $d_1=10$ cm, $d_2=15$ cm, $h=1$ cm, $l=50$ cm. The cross-sectional area $A=50\,\mathrm{cm}^2$, the length $l=50$ cm, the principal moments of area are $I_y=750\,\mathrm{cm}^4$ and $I_x=1125\,\mathrm{cm}^4$ and the warping moment of area is $I_\varpi=937.5\,\mathrm{cm}^6$. Young's modulus $E=2.1\times10^7\,\mathrm{N/cm}^2$, Shear Modulus $G=8.4\times10^6\,\mathrm{N/cm}^2$, torsional constant=polar moment of area=$J=1800\,\mathrm{cm}^4$. The rigidity ratio $e=1.5$; $K=GJl^2/(EI_w)=192$; $r^2=I_\varpi/I_y=1.25$ and $g=J/Ar^2=1800/(50\times1.25)=28.8$. The externally applied forces and moments are non-dimensionalized according to Eq. (26). We shall compare the buckling loads for various ways of torque application and give the interactive buckling surfaces for three loading parameters at a time. Finally, the results for a two-section column are shown.

As a numerical check, let $w=1$, $P=-1$, $L=1$, $M=1$, $N=1$; the displacement functions of the first nine degrees are listed in Table 4.

### 11.1. Comparison of various ways of torque application

We shall consider the effects of various ways of torque application on the buckling torque. Fig. 6 shows the interactive dynamic torque buckling curves of various ways of torque application. The heavy dash lines are the results of semi-tangential torque, the dot lines quasi-tangential torque and the solid lines uniform torque. That $P^{1/2}$ is used instead of $P$ in the axis is for more uniform spread of curves. There are two groups of curves for quasi-tangential torque. The inner pair with thick dots is for (i) $\tau^0_{zx}=-yL/I_x$ and $\tau^0_{zy}=0$ and the outer pair with slim dots is for (ii) $\tau^0_{zy}=xL/I_y$ and $\tau^0_{zx}=0$. It is observed that the quasi-tangential torque produces non-monotonic interactive buckling curves and the semi-tangential torque buckles the column in a catastrophic manner in the absence of compression. Both phenomena are unusual in the first mode of a conservative buckling problem. The uniform torque does not have any of these problems. The first buckling torque is $L=1.35$ when it

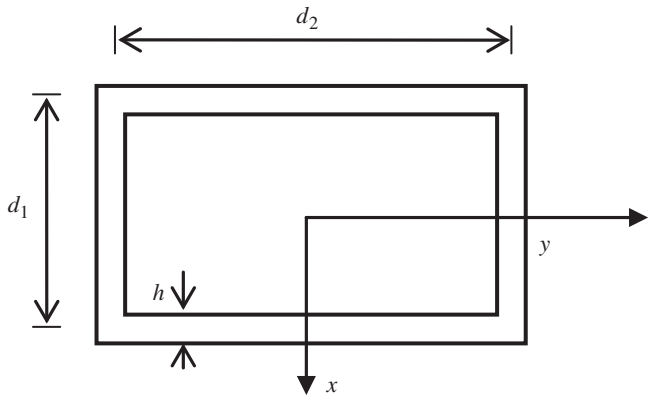


**Fig. 5.** A column having rectangular thin-walled section.

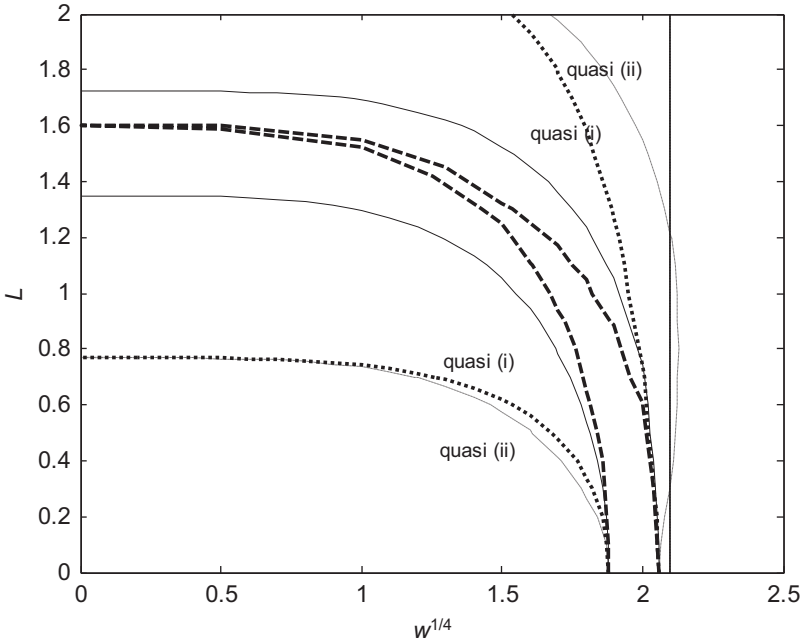


**Fig. 6.** Comparison of various ways of torque application.

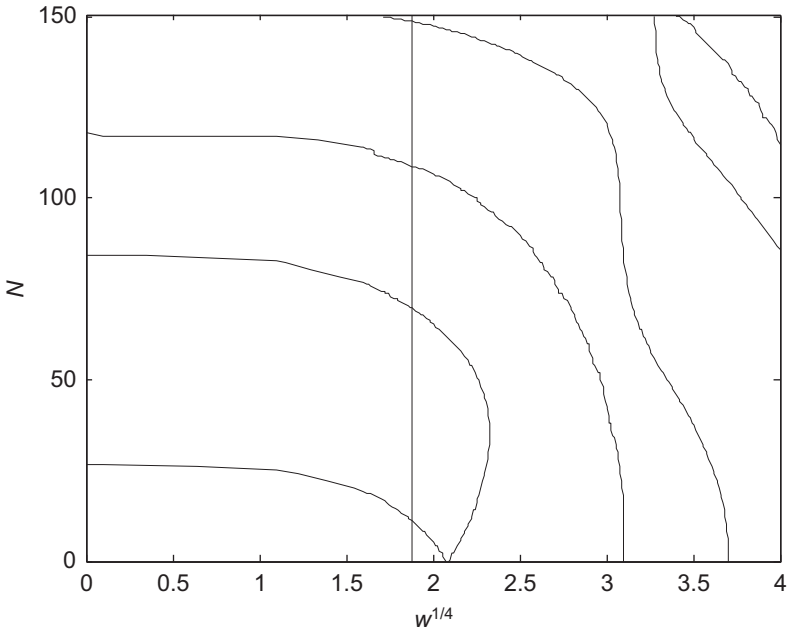


**Fig. 7.** Higher dynamic buckling $N-\omega$ modes.

applies uniformly. The quasi-tangential torque in both branches gives lower first buckling value $L=0.78$ and the semi-tangential torque over-estimates it to $L=1.56$. We have shown in Section 2 that the buckling semi-tangential torque is always twice of the buckling quasi-tangential torque. It is verified numerically here. The third mode shown vertically is not affected by the ways of torque application. We shall consider uniform torque only in the subsequent studies.

### *11.2. Higher dynamic buckling modes*

The power series method is very efficient for obtaining lower buckling modes. It can handle reasonably higher $N-\omega$ modes but fails for extremely high modes. An alternative method of Fourier $p$-elements should be used in the

later case and for non-uniform sections [16]. The first four $N-\omega$ interactive modes are plotted in Fig. 7. Since $N$ is applied along the major principal axis, it has little effect on the first bending mode along the minor principal axis showing a straight line. There are two branches emanating from the bending mode along the major axis. One is an asymmetric mode which is softened quickly by the initial moment $N$ and the other is asymmetric mode which hardened by the initial moment $N$ in the beginning. It is seen that the interactive curves loses the monotonic convexity at higher modes. Fig. 8 shows the higher interactive dynamic compression modes. The interactive curves keep the monotonic convexity even at higher modes. The power series method is numerically stable for dynamic compression buckling problems.

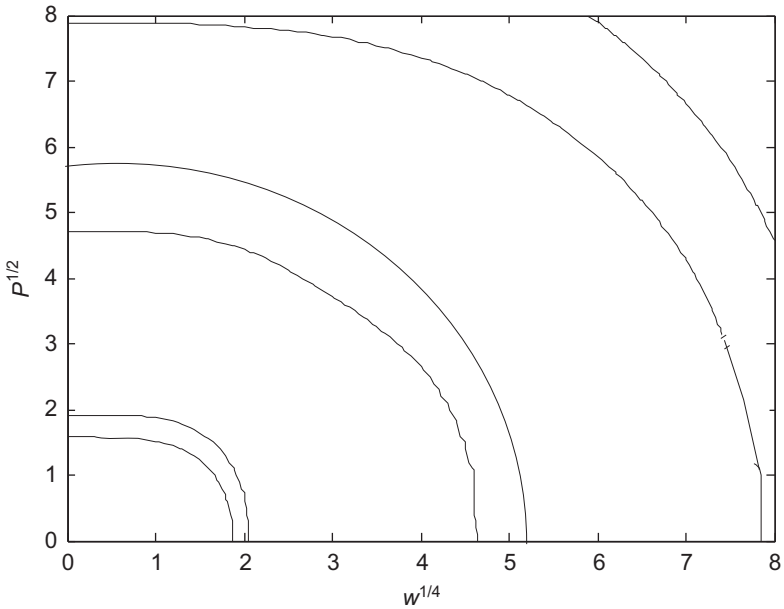


**Fig. 8.** Higher dynamic buckling $P-\omega$ modes.

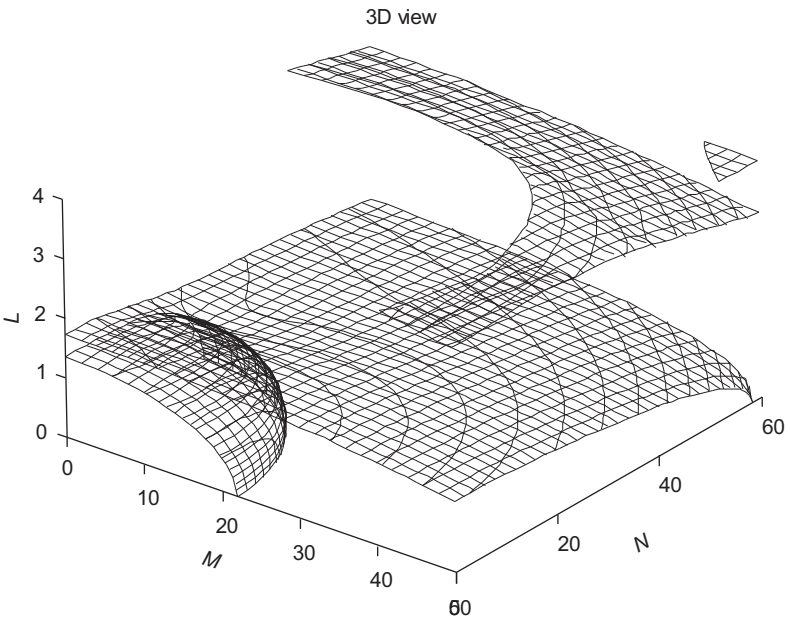


**Fig. 9.** Three-dimensional interactive buckling of moments and torque.

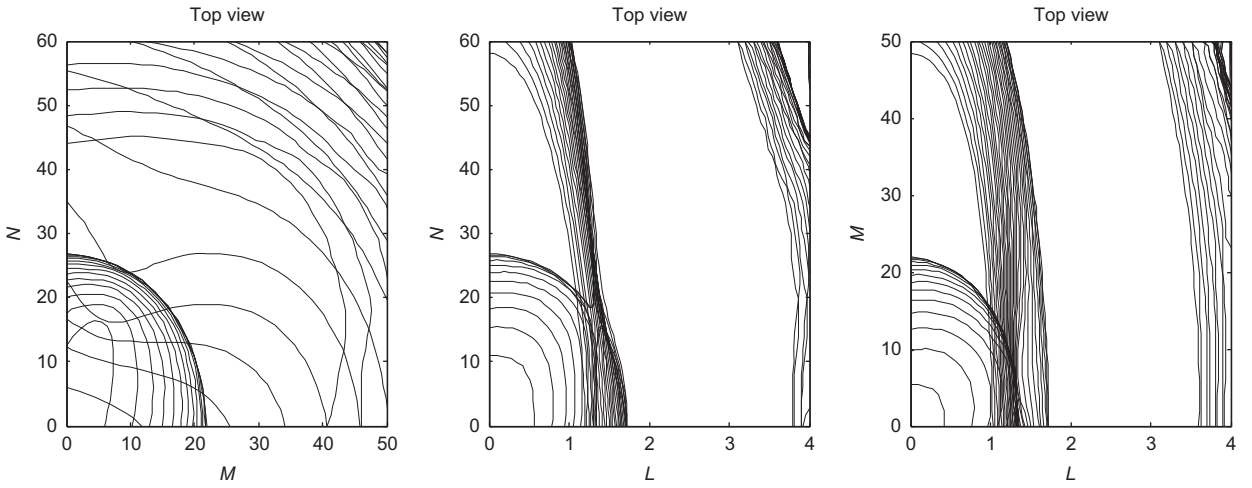


**Fig. 10.** Projections onto the *MN*, *LN* and *LM* planes.

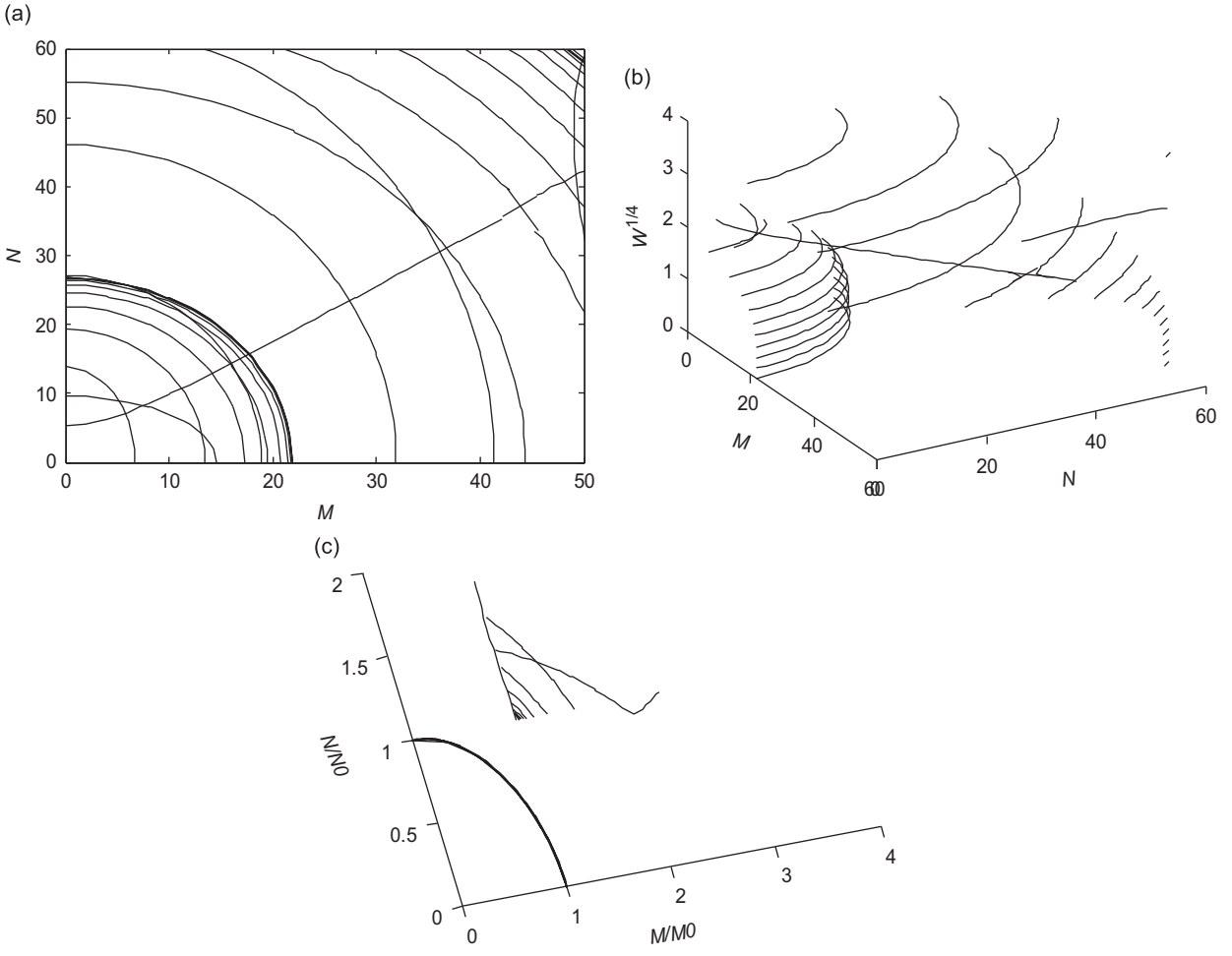


**Fig. 11.** Interactive dynamic biaxial moment buckling $L=0$: (a) top view, (b) 3D view and (c) scaled 3D view.

### 11.3. Three-dimensional interactive buckling of moments and torque

Three-dimensional interactive buckling of moments and torque is shown in Fig. 9 for the first three modes and the projections onto the *MN*, *LN* and *LM* planes are plotted in Fig. 10. The interaction surface of the first mode is convex in all directions. The second mode curves are also monotonic and convex for lower values of *L* but the convexity is lost for higher values. In fact, the second modes seem to be attracted by the first modes when they are near to each other on the same level of *L*. The attraction is more obvious if one plots the interaction curves of *L*, *N* for level values of *M*=0:2:50 in Fig. 10. A cross-over happens at about *M*=10 and a classical phenomena of avoid crossing can be observed near that value.

### 11.4. Three-dimensional interactive dynamic buckling of moments and torque

Fig. 11 shows the interactive dynamic biaxial moment buckling in the absence of initial torque *L*=0. Four modes can be observed in the three-dimensional view of Fig. 11(b). The interactive surface of the first mode is almost spherical. If one scales the level curves by the uni-axial moment buckling loads $N_0$ and $M_0$, they will be collapsed into a quarter circle if view from the top as shown in Fig. 11(c). The first mode is disappeared at $w^{1/4}=1.87$ which is the first natural vibration frequency in bending about the minor principal axis of the cantilever. The level curves for the second modes emanate from the far corner of the *MN* plane. The curves become longer for higher frequency as the portions that were outside the *MN* region move in and are disappeared at $w^{1/4}=2.07$ which is the first natural vibration frequency in bending about the major principal axis of the cantilever. The top three level curves in Fig. 11(b) are the second bending mode about the minor

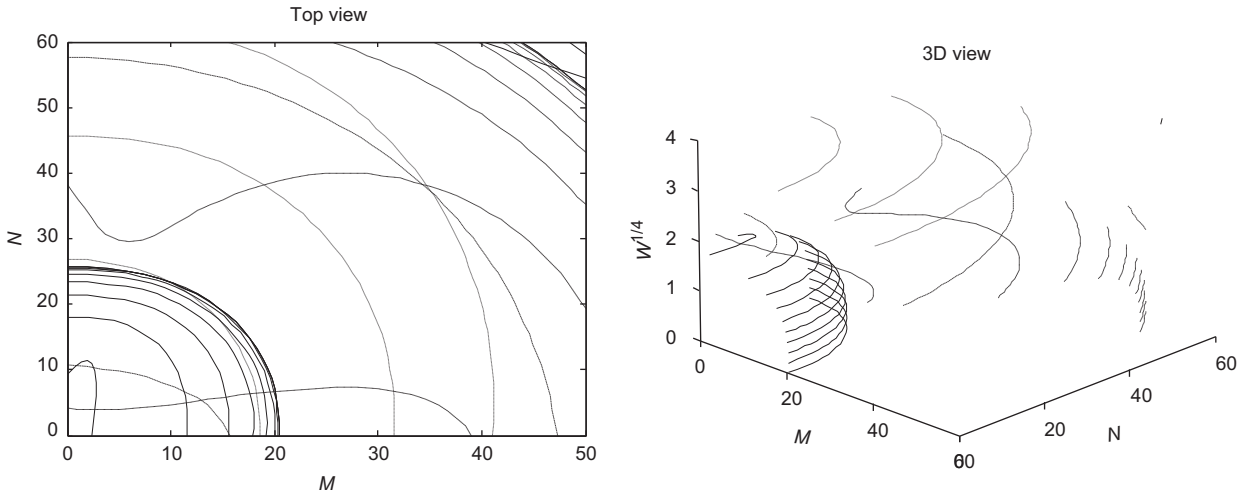


**Fig. 12.** Interactive dynamic biaxial moment buckling *L*=0.5.

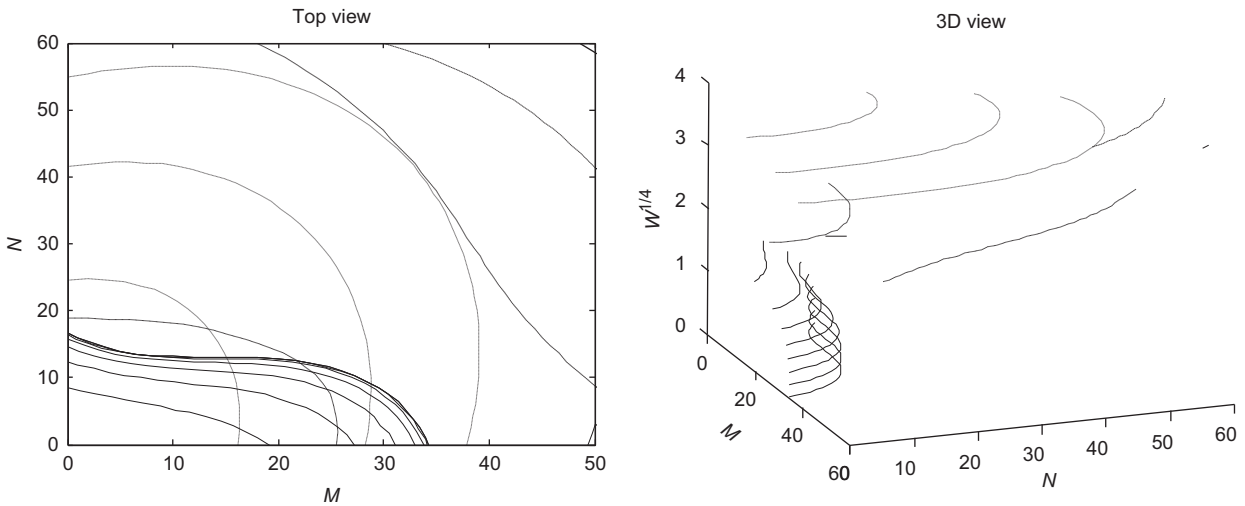


**Fig. 13.** Interactive dynamic biaxial moment buckling *L*=1.5.

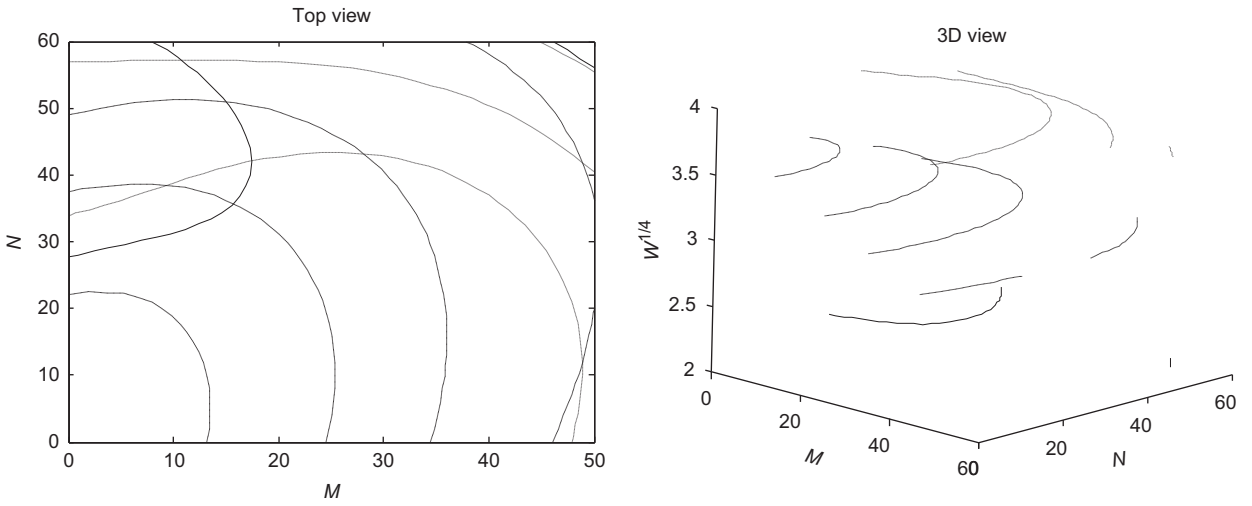


**Fig. 14.** Interactive dynamic biaxial moment buckling $L$=2.0.

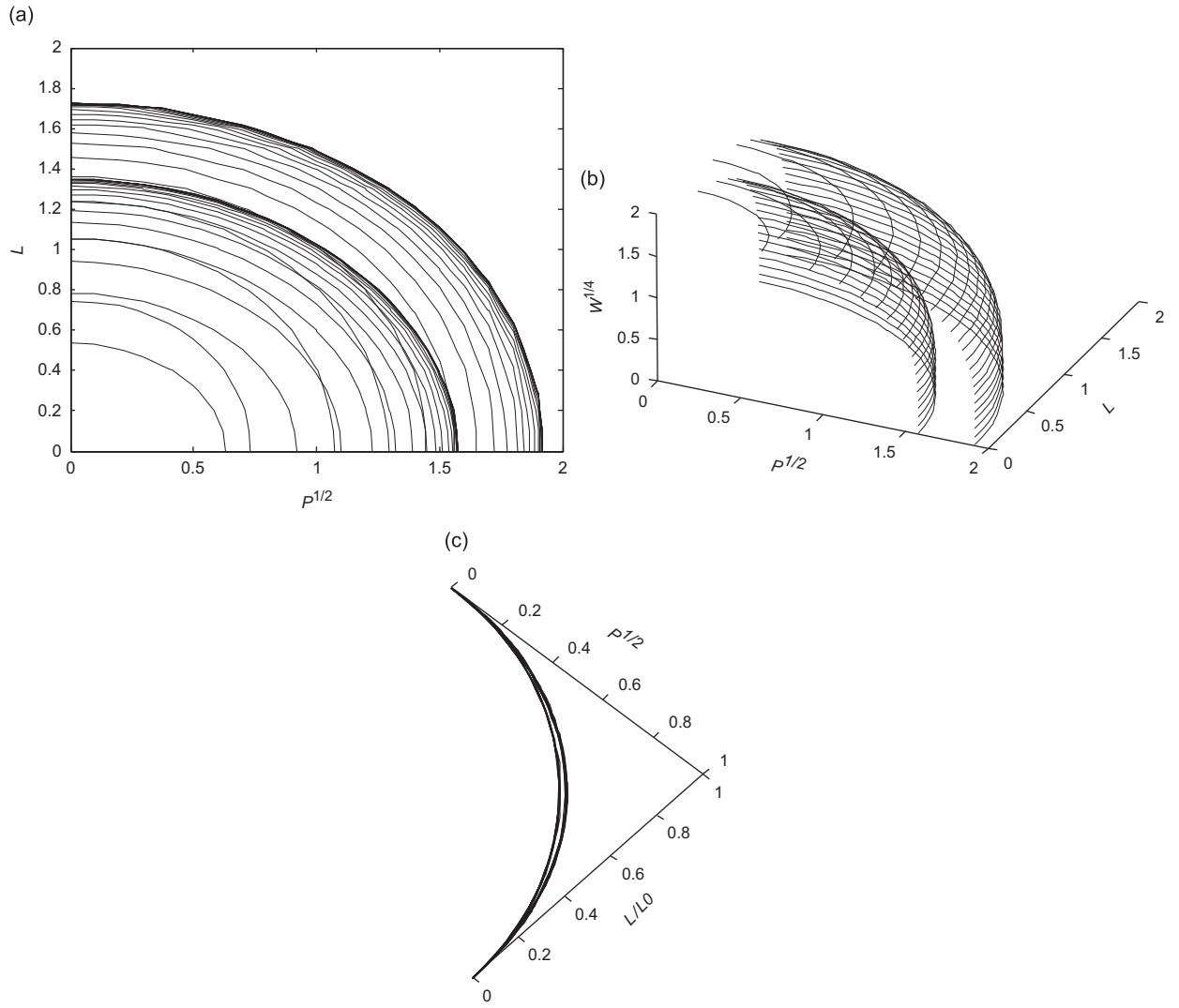


**Fig. 15.** Level curves for dynamic compression–torque buckling: (a) top view, (b) 3D view and (c) scaled 3D view.

principal axis. The level curve emanated from about $N$=10 corresponds to the torsion mode. When the uniform torque is increased, the level curves are presented in Figs. 12–14 for $L$=0.5, 1.5, 2.0, respectively. For easy explanation, we use solid lines for the lowest mode, dash lines for the second lowest and dot lines for the third lowest appearing in the figures. The first mode level curves shrink a little at $L$=0.5. Some second mode level curves are no longer convex but that of the third mode are still convex. The level curves for the first mode are completely disappeared at $L$=1.5 in Fig. 13 as the first torque buckling mode is at $L$=1.35. The level curves for the second mode are also completely disappeared at $L$=1.52 in Fig. 14 as the second torque buckling mode is at $L$=1.72.

The first two sets of interactive buckling curves under uniform torque $L$ and compression $P$ for $w^{1/4}$=0:.1:2 are plotted in Fig. 15(a) with its top view in Fig. 15(b). Both modes are monotonic and convex as usual. When the level curves are scaled by the individual buckling loads, two sets of collapsed curves of nearly circular shape are resulted as shown in Fig. 15(c).

### 11.5. Interactive dynamic buckling of moments and torque when compressed

The first three sets of interactive buckling curves under (i) uni-axial moment $M$ and compression $P$ and (ii) uni-axial moment $N$ and compression $P$ for $w^{1/4}$=0:.1:2 are plotted in Figs. 16(b) and 17(b) with their top views in Figs. 16(a) and

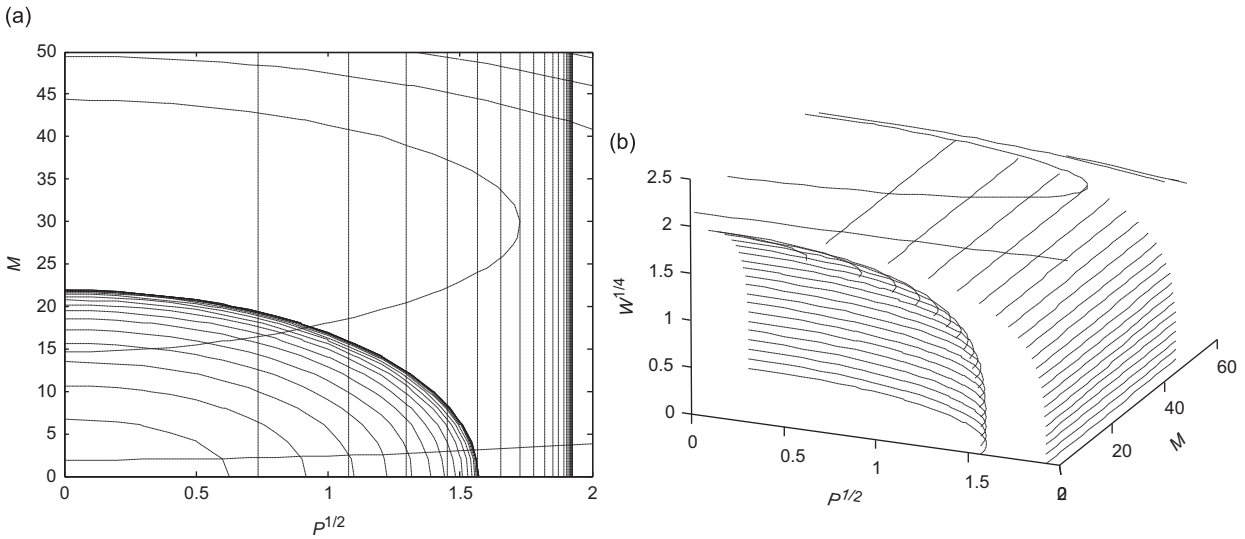


**Fig. 16.** Level curves for dynamic $M$ moment–torque buckling: (a) top view and (b) 3D view.

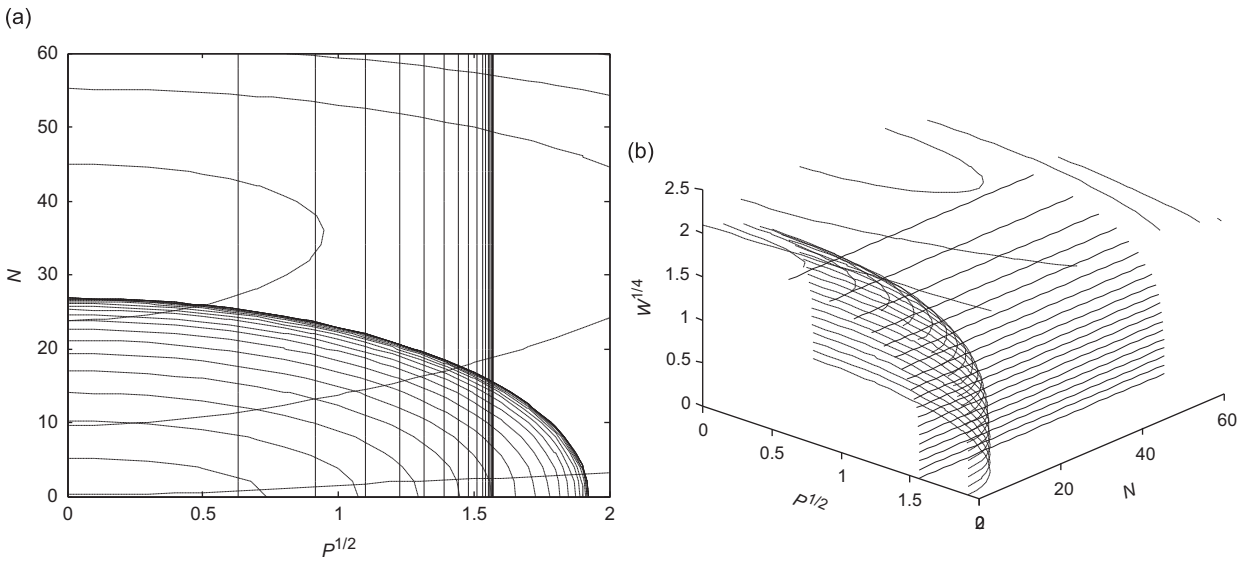


**Fig. 17.** Level curves for dynamic $N$ moment–torque buckling: (a) top view and(b) 3D view.

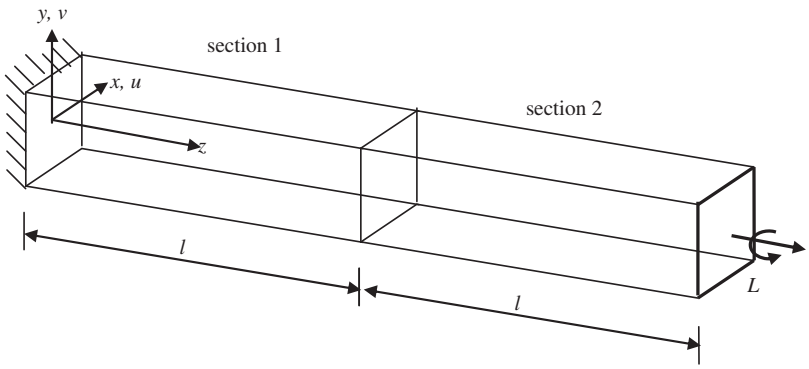


**Fig. 18.** A two-section column.

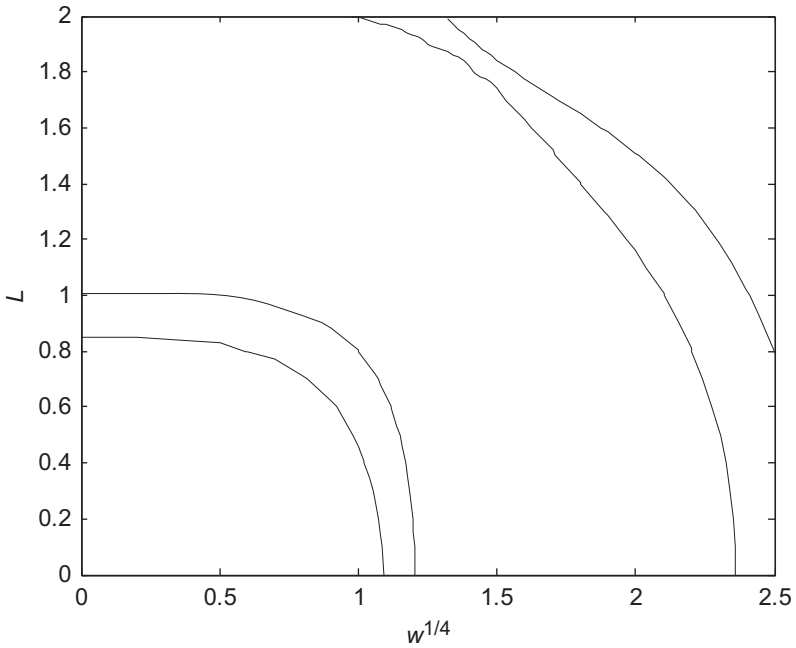


**Fig. 19.** The interactive dynamic torque buckling of a two-section column.

17(a), respectively. The first sets are monotonic and convex as usual. The second sets are rather insensitive to *M* and *N*, respectively. The third sets display some flutter like curves in the *PM* and *PN* planes, respectively, at high frequencies.

### *11.6. Interactive dynamic buckling of a two-section column*

Finally, we study the interactive dynamic torque buckling of a two-section column shown in Fig. 18. Section 1 remains the same as before. For Section 2, the thickness $h=0.5$ cm and length $l=50$ cm. All non-dimension parameters remain unchanged. The stiffness matrix will be reduced by half in value as $I_y$ is halved. After assembling, the stiffness matrix is of dimension 12. The interactive torque–compression buckling curves are shown in Fig. 19. The dash lines are modes that are rather insensitive to the apply torque.

## 12. Conclusion

The existing beam theories for torque buckling have been reviewed and suggestion to improve them is given. The buckling torques for some cases are compared with ANSYS®. Solution methods using power series are recommended. The method can provide combine dynamic buckling information when the beam is subject to end moments, end shears, axial

force and torque. Convergence requirement is discussed. Although single members have been used as examples, as the formulation is based on finite element, structural frames can be analyzed without difficulties.

## Acknowledgement

The research is fully supported by the Research Grant Council of Hong Kong Grant no. 116608.

## References

[1] Y.B. Yang, S.R. Kuo, *Theory and Analysis of Nonlinear Framed Structures*, Prentice Hall, Englewood Cliffs, NJ, 1994.
[2] H. Ziegler, *Principles of Structural Stability*, second ed., Birkhäuser, Stuttgart, Germany, 1977.
[3] J.H. Argyris, O. Hilpert, G.A. Malejannakis, D.W. Scharpf, On the geometrical stiffness matrix of a beam in space—a consistent approach, *Computational Methods in Applied Mechanics and Engineering* 20 (1979) 105–131.
[4] K. Washizu, *Variational Methods in Elasticity and Plasticity*, Pergamon, New York, 1956.
[5] A.Y.T. Leung, *The Dynamic Stiffness and Substructures*, Springer, London, 1993.
[6] M. Eisenberger, Exact static and dynamic stiffness matrices for general variable cross-section members, *AIAA Journal* 28 (6) (1990) 1105–1109.
[7] A.Y.T. Leung, W.E. Zhou, Dynamic stiffness analysis of curved thin-walled beams, *Journal of Shock and Vibration* 1 (1993) 77–88.
[8] A.Y.T. Leung, W.E. Zhou, Dynamic stiffness analysis of nonuniform Timoshenko beams, *Journal of Sound and Vibration* 181 (1995) 447–456.
[9] A.Y.T. Leung, W.E. Zhou, Dynamic stiffness analysis of axially loaded nonuniform Timoshenko columns, *Computers & Structures* 56 (1995) 577–588.
[10] A.Y.T. Leung, W.E. Zhou, Dynamic stiffness of laminated composite plates, *Thin-walled Structures* 25 (1996) 109–134.
[11] A.Y.T. Leung, W.E. Zhou, C.W. Lim, R.K.K. Yuen, U. Lee, Dynamic stiffness for piecewise non-linear Timoshenko columns by power series—part 1: conservative axial force, *International Journal for Numerical Methods in Engineering* 51 (5) (2001) 505–529.
[12] A.Y.T. Leung, W.E. Zhou, C.W. Lim, R.K.K. Yuen, U. Lee, Dynamic stiffness for piecewise non-linear Timoshenko columns by power series—part 2: follower force, *International Journal for Numerical Methods in Engineering* 51 (5) (2001) 531–552.
[13] Z. Bin, A.Y.T. Leung, Dynamic stiffness for thin-walled structures by power series, *Journal of Zhejiang University Science A* 7 (8) (2006) 1351–1357.
[14] A. Simpson, On the solution of $S(\omega)=0$ by a Newtonian procedure, *Journal of Sound and Vibration* 97 (1984) 153–164.
[15] T.H. Richards, Y.T. Leung, An accurate method in structural vibration analysis, *Journal of Sound and Vibration* 55 (1977) 363–376.
[16] B. Zhu, A.Y.T. Leung, Fourier p-elements for curved beam vibrations, *Thin-Walled Structures* 42 (1) (2004) 39–57.
[17] A.Y.T. Leung, An accurate method of dynamic condensation in structural analysis, *International Journal for Numerical Methods in Engineering* 12 (1978) 1705–1716.
[18] A.Y.T. Leung, An accurate method of dynamic substructuring with simplified computation, *International Journal for Numerical Methods in Engineering* 14 (1979) 1241–1256.
[19] C.D. Eick, M.P. Mignolet, Vibration and buckling of flexible rotating beams, *AIAA Journal* 33 (3) (1995) 528–538.
[20] S.K. Sinha, On-linear dynamic response of a rotating radial Timoshenko beam with periodic pulse loading at the free-end, *International Journal of Non-linear Mechanics* 40 (2005) 113–149.
[21] A. Paolone, M. Vasta, A. Luongo, Flexural–torsional bifurcations of a cantilever beam under potential and circulatory forces I. Non-linear model and Stability analysis, *International Journal of Non-linear Mechanics* 41 (2006) 586–594.
[22] S.K. Sinha, Combined torsional–bending–axial dynamics of twisted rotating cantilever beam with contact-impact loads at the free-end, *ASME Journal of Applied Mechanics* 74 (2007) 505–522.